



THE HONG KONG
POLYTECHNIC UNIVERSITY

香港理工大學

Pao Yue-kong Library

包玉剛圖書館

Copyright Undertaking

This thesis is protected by copyright, with all rights reserved.

By reading and using the thesis, the reader understands and agrees to the following terms:

1. The reader will abide by the rules and legal ordinances governing copyright regarding the use of the thesis.
2. The reader will use the thesis for the purpose of research or private study only and not for distribution or further reproduction or any other purpose.
3. The reader agrees to indemnify and hold the University harmless from and against any loss, damage, cost, liability or expenses arising from copyright infringement or unauthorized usage.

IMPORTANT

If you have reasons to believe that any materials in this thesis are deemed not suitable to be distributed in this form, or a copyright owner having difficulty with the material being included in our database, please contact lbsys@polyu.edu.hk providing details. The Library will look into your claim and consider taking remedial action upon receipt of the written requests.

DESIGN AND CONTROL OF A SOFT
AERIAL VEHICLE FOR CONDUCTING
AERIAL GRASPING

CHEUNG HIU CHING

MPhil

The Hong Kong Polytechnic University

2025

The Hong Kong Polytechnic University

Department of Aeronautical and Aviation Engineering

**Design and Control of a Soft Aerial Vehicle for
Conducting Aerial Grasping**

Cheung Hiu Ching

A thesis submitted in partial fulfilment of the requirements of the degree of
Master of Philosophy

August 2024

CERTIFICATE OF ORIGINALITY

I hereby declare that this thesis is my own work and that, to the best of my knowledge and belief, it reproduces no material previously published or written, nor material that has been accepted for the award of any other degree or diploma, except where due acknowledgement has been made in the text.

Cheung Hiu Ching

Abstract

Unmanned aerial vehicles (UAVs) have gained significant attention because of their potential applications across various industries, including search and rescue, harvesting, and drone delivery. The practical grasping and landing abilities of these aerial robots can guarantee a high success rate in their missions. To improve the grasping performance of UAVs, this thesis introduces a novel modular pneumatic soft gripper design tailored explicitly for aerial grasping of various target objects. Compared to the traditional rigid gripper, the proposed soft gripper aims to act as a shock absorber that can dampen the impact force induced during aerial grasping.

The soft gripper can grasp and release the target items through inflation and deflation. The flexibility of the pneumatic soft gripper allows deflation to reach its opening, providing higher grasping tolerance than the traditional rigid gripper. Moreover, the softness of the soft gripper makes it capable of grasping objects without any damage through inflation. Modular connectors of the soft fingers offer two configurations for this 4-tip soft gripper, H-base (cylindrical) and X-base (spherical), allowing adaptability to different target objects. The airflow of the soft gripper is controlled by its two solenoid valves, while a feed-forward proportional controller of an air pump manages the pressure regulation.

In addition to the above, a soft aerial vehicle (SAV) with a quadrotor and the proposed soft gripper is proposed. An onboard computer of the SAV can command the soft gripper's airflow control system and pressure regulation directly to ensure aerial grasping efficiency. The soft gripper is installed under the centre of gravity of the SAV to serve as a soft landing

gear when deflated, eliminating the requirement for additional landing gear. Hence, this soft landing design reduces the net weight of the SAV and simplifies aerial manipulation control by removing the extra landing gear control.

Nevertheless, controlling the dynamics of UAVs during their aerial grasping mission is challenging. The increased mass from the payload adversely impacts their thrust prediction, while unpredictable environmental disturbances further complicate control efforts. Thus, this thesis aims to enhance the control of the SAV during aerial grasping by integrating a disturbance observer into a Nonlinear Model Predictive Control (NMPC). This incorporation compensates for dynamic model idealization and uncertainties arising from the additional payloads and unpredictable disturbances. Hence, the Disturbance Observer-based Nonlinear Model Predictive Control (DOMPC) can effectively minimize tracking errors and enable precise aerial grasping along all three axes.

The proposed disturbance observer utilises an Extended Kalman Filter (EKF) to estimate the linear acceleration disturbances of the SAV. The suggested SAV equipped with DOMPC demonstrates remarkable performance in carrying both static and non-static payloads, leading to the successful grasping of different objects with various mass distributions. Notably, the SAV also achieves an impressive payload-to-weight ratio in its payload test in mid-air, surpassing previous investigations in soft grasping.

Publications Arising from the Thesis

- [1] C.-W. Chang, L.-Y. Lo, **H. C. Cheung**, Y. Feng, A.-S. Yang, C.-Y. Wen, and W. Zhou, “Proactive guidance for accurate uav landing on a dynamic platform: A visual–inertial approach,” *Sensors*, vol. 22, no. 1, p. 404, 2022.
- [2] **H. C. Cheung**, C.-W. Chang, B. Jiang, C.-Y. Wen, and H. K. Chu, “A modular pneumatic soft gripper design for aerial grasping and landing,” in *2024 IEEE 7th International Conference on Soft Robotics (RoboSoft)*, 2024, pp. 82–88.
- [3] **H. C. Cheung**, B. Jiang, Y. Hu, H. K. Chu, C.-Y. Wen, and C.-W. Chang, "Aerial Grasping with Soft Aerial Vehicle Using Disturbance Observer-Based Model Predictive Control," (to be resubmitted to *IEEE Robotics and Automation Letters*) 2024. [Online].

Available: <https://arxiv.org/abs/2409.14115>

Acknowledgements

I would like to express my heartfelt gratitude to my supervisor, Professor Chih-yung Wen, for his unwavering guidance and support throughout my MPhil journey. His expertise and encouragement have been invaluable to my academic and personal growth. His insightful feedback and innovative approach to problem-solving have been crucial in navigating my research challenges.

I am also deeply thankful to my co-supervisor, Dr. Kar Hang, Henry Chu, for his insightful advice and patience. His mentorship has been instrumental in shaping my research and refining my skills. His encouragement to explore new ideas and perspectives has enriched my academic journey.

I am privileged to work alongside my talented teammates, Bailun Jiang, Yang Hu, Yefeng Yang, and Li-yu Lo, as well as the entire PolyU AIRO Lab. Their generosity and thoughtfulness have made my research experience truly enriching and inspiring.

Moreover, I sincerely appreciate my senior, Ching-wei Chang, for sharing his professional expertise in mechatronics. His insightful comments on my research publication have greatly enhanced my technical capabilities and academic perspective.

Lastly, I am profoundly grateful to my family for their unwavering support and encouragement and to all my friends who have stood by me. Your belief in me has been a constant source of strength and motivation.

Contents

Abstract	II
Publications Arising from the Thesis	IV
Acknowledgements	V
List of Figures	XIV
List of Tables	XV
List of Abbreviations	XVI
1 Introduction	1
1.1 Background	1
1.2 Motivation	2
1.2.1 Modular Pneumatic Soft Gripper for Aerial Grasping	2
1.2.2 Simplification of landing mechanism for Aerial Grasping	4
1.2.3 Disturbance Observer-based Controller for Aerial Grasping Control	4
1.3 Contribution	5
1.4 Outline of the Thesis	7
2 Literature Review	10
2.1 Soft Gripper Applications on Unmanned Aerial Vehicles	10

2.1.1	Tendon-actuated Soft Gripper Design and Control	10
2.1.2	Pneumatic Soft Gripper Design and Control	12
2.1.3	Comparison of Tendon-actuated Soft Grippers and Pneumatic Soft Grippers	15
2.2	Aerial Grasping System and Control	16
2.2.1	Rigid Aerial Grasping System and Control	16
2.2.2	Soft Aerial Grasping System and Control	18
2.2.3	Comparison of Aerial Grasping with Soft Gripper and Rigid Gripper	21
3	Modular Soft Gripper Design and Control	22
3.1	Mechanical Design	22
3.1.1	Structure of Pneumatic Soft Gripper Without Inextensible Layers .	23
3.1.2	Structure of Pneumatic Soft Gripper With Inextensible Layers . . .	24
3.2	Fabrication	25
3.2.1	Details of Pneumatic Soft Gripper Without Inextensible Layers . .	25
3.2.2	Details of Pneumatic Soft Gripper With Inextensible Layers)	26
3.3	Electronics	28
3.4	Control of Soft Gripper	29
3.4.1	Airflow Control System	29
3.4.2	Air pump Regulation	31
3.5	Static Grasping Test	35
3.5.1	Results of Pneumatic Soft Gripper Without Inextensible Layers . .	35
3.5.2	Results of Pneumatic Soft Gripper With Inextensible Layers	38
3.5.3	Comparison of the Results of the X-base and H-base Soft gripper .	39
4	Soft Aerial Vehicle Design and Control	40
4.1	Overall System Design	40
4.2	System Dynamics	41

4.3	Disturbance Observer Design	43
4.3.1	Disturbance Observer Using an Extended Kalman Filter	44
4.3.2	Disturbance Observer Using a Three-order Robust Differentiator	47
4.3.3	Observers Performance Test	49
4.4	Disturbance Observer-Based Nonlinear Model Predictive Control	51
4.4.1	Controller adaptability Test	54
4.5	Finite State Machine for Aerial Grasping mission	56
4.5.1	First stage: Takeoff and waiting for position data of target object	56
4.5.2	Second stage: Approaching the target object	58
4.5.3	Third stage: Grasping the target object at the desired grasp point	58
4.5.4	Forth stage: Lifting the target object object to a desired hovering point	59
4.5.5	Fifth stage: Releasing the target object at the releasing destination	59
4.5.6	Sixth stage: Landing	59
4.6	Payload Test	60
4.6.1	Position Tracking Results of SAV with H-base Soft Gripper (With Inextensible Layer)	61
4.6.2	Position Tracking Results of SAV with X-base Soft Gripper (With Inextensible Layer)	63
4.7	Soft Aerial Grasping Test	64
4.8	Soft Landing Test	70
4.8.1	Results of Soft Gripper Without Inextensible Layers	71
4.8.2	Results of Soft Gripper With Inextensible Layers	72
5	Conclusion and Future Work	73
5.1	Conclusion	73
5.2	Future works	74

6 Appendices	76
6.1 Video of Static Grasping	76
6.2 Video of Payload Test	77
6.3 Video of Aerial Grasping	77
6.4 Video of Soft Landing	78
6.5 Open-source Materials (GitHub)	79
Bibliography	80

List of Figures

1.1	Prototype of the proposed soft aerial vehicle (with H-base soft gripper (left) or X-base soft gripper (right)).	6
2.1	Images with (a) a bio-inspired tendon-actuated soft gripper [1], (b) a tendon-actuated soft landing gear [2], (c) a soft tendon-actuated gripper for dynamic grasping [3], and (d) a modular soft tendon-actuated gripper [4]. . .	13
2.2	Images with (a) a pneumatic soft gripper with inextensible layers [5], (b) a lightweight wearable pneumatic gripper [6], (c) a three-finger pneumatic soft gripper [7], and (d) a pneumatic soft gripper with inextensible layers and semi-circular polymer rings [8].	15
2.3	Images with (a) an aerial harvesting system by a rigid gripper [9], (b) a perching system by a rigid gripper [10], (c) aerial grasping of a suspending object with a rigid gripper [11], and (d) rigid aerial grasping by unactuated hinges of a quadrotor [12].	18
2.4	Images with (a) dynamic grasping [3], (b) a soft drone with onboard perception [4], (c) soft drone with a pneumatic gripper and a rigid landing gear [7], and (d) soft drone with a robot arm that contains a soft pneumatic gripper [8].	20

3.1	Dimensions of the X-base (spherical) soft gripper when it is (a) initially opened, (b) fully opened, and (c) fully closed. And the dimensions of the H-base (cylindrical) soft gripper when it is (d) initially opened, (e) fully opened, and (f) fully closed.	23
3.2	Dimensions of the X-base (spherical) soft gripper when it is (a) initially opened, (b) fully opened, and (c) fully closed. And the dimensions of the H-base (cylindrical) soft gripper when it is (d) initially opened, (e) fully opened, and (f) fully closed.	24
3.3	The exploded view (a) and assembly (b) of the mould of the soft finger's main body. The exploded view (c) and assembly (d) of the mould of the soft finger's cover. (e) The side view of the soft gripper.	25
3.4	The exploded view (a) and assembly (b) of the mould of the soft finger's main body. The exploded view (c) and assembly (d) of the mould of the soft finger's cover. (e) The side view of a soft gripper. The exploded view (f) and assembly (g) of the mould of the back of the soft finger.	27
3.5	Moulds for adhering the soft finger with an inextensible layer: (a) isometric view and (b) side view.	27
3.6	The exploded view of the electronics of the soft gripper with weight information.	29
3.7	Airflow of the soft gripper's system.	30
3.8	Block diagram of feed-forward proportional control of the soft gripper. . . .	31
3.9	Comparison between feed-forward proportional controller and proportional controller of the soft gripper.	34
3.10	Tested Object Set: (a) Pen Holder with Loads, (b) Computer Mouse, (c) Double-sided Tape, (d) Pen, (e) Spray Paint, (f) Syringe, (g) Membership Card, (h) Pocket Tissue Paper, (i) Spherical Container with Loads, (j) Plastic Box.	36

3.11	Grasping success rate results of 2 configurations. *The X-base gripper can hang and wrap the tape, while the H-base gripper always wraps the tape. .	37
3.12	Examples of grasping tests: Grasping (a) a pen holder with 270 g loads and (b) a spherical container with 160 g loads by an X-base gripper; Grasping (c) a computer mouse and (d) a can of spray paint with an H-base gripper.	37
3.13	Demonstration of grasping (a) a 409 g plastic beaker with three roll rulers by an X-base gripper and (b) a 342 g lead-free circuit board cleaner with an H-base gripper.	38
4.1	3D CAD drawing of the exploded view of the proposed Soft aerial vehicle (SAV).	41
4.2	SAV sketch with its inertial frame Γ_I and body frame Γ_B	42
4.3	Trajectories results of the SAV lemniscate flights under the application of NMPC-EKF and NMPC-RD3.	50
4.4	Position tracking performance of the SAV Lemniscate flights with an additional 257g load using NMPC-EKF and NMPC-RD3 along the x, y, and z axes.	50
4.5	A 257 g off-centered load is placed next to the battery of the SAV. The distance between the center of the SAV and the center of the load is 35 mm.	51
4.6	Cascaded loop control structure of disturbance observer-based Nonlinear model predictive control (NMPC) (Disturbance observer-based nonlinear model predictive control (DOMPC)).	52
4.7	Position tracking performance of the SAV circular flights with an additional 257g load using DOMPC, NMPC, and Proportion-Integration-Differentiation (PID) along the x, y, and z axes.	55
4.8	Trajectories results of the SAV circular flights.	55
4.9	Finite state machine diagram for the SAV aerial grasping task.	57
4.10	Trajectory of the aerial grasping mission.	57

4.11 Payload test of the SAV with its soft gripper (without inextensible layers): hovering after holding a 217 g payload in total with its (a) X-base and (b) H-base soft gripper, respectively.	60
4.12 Payload test of the SAV with its soft gripper (with inextensible layers): (a) hovering after carrying a 634 g payload in total with its H-base soft gripper. (b) hovering after carrying a 481 g payload in total with its X-base soft gripper.	61
4.13 Position tracking performance along the x, y, and z axes in the payload test of the SAV with its H-base soft gripper.	62
4.14 Position tracking performance along the x, y, and z axes in the payload test of the SAV with its X-base soft gripper.	63
4.15 Grasping pipeline overview of the proposed soft aerial grasping.	64
4.16 Three target objects: (a) Spherical container with loads. (b) Shuttlecock tube with its slide loads. (c) Plastic bottle with dyed water	65
4.17 Trajectories of grasping the three targets.	66
4.18 Position tracking errors during the process of grasping the three different target objects (the dotted lines depict the time of SAV started to lift the objects after grasping).	67
4.19 Disturbance results from grasping the three different target objects (the dotted lines depict the time of SAV started to lift the objects after grasping).	69
4.20 Standard landing test with (a) the H-base soft gripper and (b) the X-base soft gripper, and tilt landing test with the (c) X-base and (d) H-base soft gripper.	71
4.21 Standard landing with (a) the H-base soft gripper and (b) the X-base soft gripper, and landing with two soft fingers of the (c) H-base and (d) X-base soft gripper.	72
6.1 QR code for the video of the static grasping test by the soft gripper.	76

6.2 QR code for the video of SAV’s payload test. 77

6.3 QR code for the SAV’s aerial grasping test video. 77

6.4 QR code for the video of soft landing. 78

List of Tables

1.1	Payload-to-weight ratio of the proposed SAV with the soft gripper consists of inextensible layers and the previous investigations.	8
2.1	Comparison of tendon-actuated soft gripper and pneumatic soft gripper. . .	16
2.2	Comparison of aerial grasping with soft gripper and rigid gripper.	21
3.1	Parameters in air pump regulation.	33
3.2	Comparison of the Results of the X-base and H-base Soft gripper.	39
4.1	Dimensions and weights of target objects.	65
4.2	Comparison of SAV aerial grasping performance with the three target objects.	69
4.3	Comparison of SAV landing performance on ground and tilt platform. . . .	72

List of Abbreviations

ACADO Automatic control and dynamic optimization

DOMPC Disturbance observer-based nonlinear model predictive control

DOF Degrees of freedom

EKF Extended Kalman filter

FCU Flight control unit

FSM Finite state machine

GNSS Global navigation satellite system

IMU Inital measurement unit

MPC Model predictive control

NMPC Nonlinear model predictive control

OCP Optimal control problem

PCB Printed circuit board

PID Proportion-Integration-Differentiation

PLA Polylactic acid

PWM Pulse-width modulation

XVI

QP Quadratic programming

RD3 Three-order robust differentiator

RK4 4th-order Runge-Kutta

ROS Robot operating system

RTK real time kinematics

SAV Soft aerial vehicle

TPU Thermoplastic polyurethane

UAV Unmanned aerial vehicle

Chapter 1

Introduction

1.1 Background

Unmanned aerial vehicle (UAV) has been extensively investigated in various applications, such as building inspection [13], surveillance [14], drone delivery [15], search and rescue [16], and harvesting [17]. Drones are capable of performing automatic tasks with high-agile manoeuvres due to their simple aerodynamics model and mechanical structure, which offer advantages over fixed-wing UAVs [18]. The versatility and ease of manoeuvrability of quadrotors allow them to adapt to complex environments across multiple industries.

Recently, aerial grasping has been a rapidly growing area of research in autonomous systems, particularly because of its potential applications in drone delivery. These aerial grasping applications include several aspects such as food delivery [19], medical goods delivery [20], search and rescue [21], and environmental cleaning [22]. The drone delivery industry prioritizes goods safety and operational efficiency to ensure successful and reliable services. In Hong Kong, for instance, recent regulation on small unmanned aircraft [23] highlights the government's increasing concern for aerial vehicle safety, reflecting broader global trends.

According to these developments, this thesis would like to enhance drone delivery

systems by improving the safety and efficiency of UAV operations. Specifically, the gripper design of the drone delivery system will be optimized to ensure the safety of the goods, and the aerial grasping control system will be designed to securely handle various goods without compromising flight performance. This thesis focuses on improving the payload-to-weight ratio of the aerial grasping system and minimising tracking errors during the aerial grasping tasks.

A higher payload-to-weight ratio is crucial for drone systems to enhance payload capacity. However, heavier payloads increase the thrust propulsion burden on drones. This thesis aims to introduce an innovative lightweight gripper that maintains satisfactory payload capability, balancing efficiency and performance. By optimizing the gripper design, overall drone operations can be improved without compromising on payload handling.

Another foreseen challenge in aerial grasping systems is reducing flight tracking errors after a successful grasp. Once the UAV's payload is grabbed, its total mass rapidly increases. This impact will be more significant when the payload-to-weight ratio is improved. Thus, the thesis aims to present an aerial grasping control method that accounts for all disturbances during the mission, ensuring stability and precision in UAV grasping operations.

1.2 Motivation

1.2.1 Modular Pneumatic Soft Gripper for Aerial Grasping

Soft grippers offer a promising alternative to rigid grippers due to their simplified control systems, reduced complexity, and excellent force absorption capabilities. During grasping, complicated controls and instability caused by a rigid gripper design are mentioned in [24]. Also, the complex mechanism of the rigid gripper increases the difficulties of fabricating

a Unmanned aerial vehicle (UAV) with the rigid gripper. To tackle several disadvantages of the traditional UAV's gripper, a soft gripper is proposed to replace the rigid one to overcome the control difficulties and the number of additional components. To leverage the principles of soft robotics, these lightweight and controllable mechanisms provide stability during grasping by dampening impact forces [25–27]. Their flexibility allows for a broader range of object dimensions, increasing grasping tolerance.

Since the soft gripper can be much more deformable than the rigid one, it can dampen the impact forces during grasping and provide higher grasping tolerance. Thus, the soft gripper approach can increase the flight stability of the grasping and prevent damage to the goods. Besides, since the gripper is soft and flexible, the dimensions and shapes of the goods will not be constrained as much as using a rigid gripper.

Generally, most of the UAVs without an additional robot arm can grasp their target object by hovering above the object to ensure the location of the grasping point is correct [12,28]. Those consisting of the robot arm with a gripper can grasp the object by changing the poses of the robot arms to grasp the object in mid-air [29]. To reduce the control difficulty and grasping position errors, the UAV tries to keep hovering horizontally during grasping with its robot arm and gripper [30,31]. Since this thesis focuses on maximizing the payload-to-weight ratio, the suggested soft aerial grasping system gets rid of the robot arm design to ensure a low net weight. Referring to the existing aerial grasping systems above, the proposed quadrotor aims to provide robust aerial grasping by hovering over the target objects with its soft gripper.

To simplify the grasping motion and avoid the complicated control of the infinite Degrees of freedom (DOF) of soft robotics, a pneumatic soft gripper with four soft fingers that can inflate or deflate all the fingers simultaneously is suggested [32]. The gripper opens itself by deflating all fingers to let the fingers move outwards of the centre of the gripper. Similarly, the gripper grasps the object by inflating its fingers to move inwards. Since a robot arm is not included, the proposed soft gripper is located beneath the centre

of gravity of the UAV and securely grasps different target objects by controlling inflation and deflation. The soft gripper guarantees the goods' safety based on its impact force dampening capability and improves grasping efficiency through its simple airflow control.

1.2.2 Simplification of landing mechanism for Aerial Grasping

Replacing the rigid landing gear with the proposed soft gripper as the landing mechanism enhances the capability of aerial manipulation for the Soft aerial vehicle (SAV) [3]. It eliminates the need for additional actuators and simplifies the control system by excluding the complicated operations of the landing gear adjustment during takeoff, landing, and grasping.

The soft gripper deflates during takeoff and landing as soft landing gear, capable of supporting the quadrotor before takeoff and dampening the contact force of the quadrotor and the ground during landing. Consequently, the soft gripper can provide grasping and landing services with the same airflow control system and pressure regulation. This approach can significantly minimize the net weight of the whole aerial grasping system and the complexity of the gripper's control.

1.2.3 Disturbance Observer-based Controller for Aerial Grasping Control

Model predictive control (MPC) of a UAV is widely used to ensure flight stability and robustness in UAVs [33–36]. Based on a receding horizon principle, this optimal feedback control technique considers the system model. With the dynamic model of the system, MPC can optimize the control inputs over a future time horizon. [37] presented modelling, controller design, and implementation of MPC for a quadrotor UAV. The controller is in-

tegrated with Robot operating system (ROS) and implemented in a cascading approach. In this work, both the linear MPC and Nonlinear model predictive control (NMPC) were developed, and their performances were compared. In general, linear MPC demonstrated a common drawback of linear controllers, which is failing to consider the system's nonlinearity and leading to substantial tracking errors in operations involving aggressive manoeuvres. Consequently, NMPC is selected for the proposed SAV control because of its superior tracking performance despite its higher computational demands [32].

To eliminate the disturbances during aerial grasping, this thesis aims to improve SAV control by adding a disturbance observer into the NMPC controller [38]. This addresses dynamic changes, additional payload effects, and unpredictable disturbances. By integrating the proposed disturbance observer into the developed NMPC SAV controller [32, 39, 40], dynamic model idealization can be compensated and the uncertainties can be handled too. Combining disturbance observer-based NMPC with the SAV controller, the suggested soft aerial grasping system minimizes tracking errors along three axes and enables precise aerial grasping.

1.3 Contribution

The proposed Unmanned aerial vehicle (UAV) represents a significant advancement by combining lightweight modular construction with the capability for aerial grasping [32, 38]. It is capable of autonomous aerial grasping and landing, utilising a lightweight modular pneumatic soft gripper. By incorporating a feed-forward proportional controller, precise pressure regulation can be ensured for the soft gripper control. The suggested soft gripper also functions as a soft landing gear when it deflates during takeoff and landing. This novel design eliminates the need for an extra landing gear to simplify the UAV's control complexity, resulting in a more streamlined aerial grasping system. Furthermore, the soft gripper can grasp various objects with different shapes and weights by its two

configurations, providing an efficient grasping capability.



Figure 1.1: Prototype of the proposed soft aerial vehicle (with H-base soft gripper (left) or X-base soft gripper (right)).

Additionally, to consider the external disturbances caused by the unknown weights of payloads and unpredictable environmental disturbances, a Nonlinear model predictive control (NMPC) controller based on a disturbance observer is proposed to operate the UAV for its aerial grasping mission. Using Extended Kalman filter (EKF), the designed disturbance observer can adapt to the UAV's dynamic model changes throughout the complete aerial grasping task. As a result, this suggested aerial grasping control system provides a satisfactory payload-to-weight ratio compared to existing works.

The main contributions of the thesis are summarised as follows.

- The integration of modular connectors reduces the soft gripper's configuration time and the soft fingers' fabrication time [32]. With just four soft fingers, the gripper can be arranged into two configurations, providing a versatile range of options for grasping target objects based on their shapes. The X-base soft gripper can grasp spherical or rounded objects, while cylindrical or rectangular objects can be grasped by the H-base soft gripper. This modularity enhances the gripper's adaptability to grasp various objects during aerial grasping operations.
- The dual capabilities of the soft gripper serve as both a grasping mechanism and a landing gear [32]. The deflation of the soft gripper enables it to function as a soft

landing gear, obviating the need for an additional rigid landing gear to reduce the net weight of the Soft aerial vehicle (SAV). This weight reduction improves flight efficiency and simplifies the complexity associated with aerial operation control.

- The proposed Disturbance observer-based nonlinear model predictive control (DOMPC) for soft aerial grasping compensates for dynamic changes caused by payload weight and other uncertainties [38]. By utilising EKF to fuse Initial measurement unit (IMU) data from the Flight control unit (FCU) and incorporating position and velocity information for validation, the estimated linear acceleration disturbances can be integrated into the existing NMPC [32] for improved control of the SAV.
- The proposed SAV equipped with the DOMPC is capable of handling both static and non-static payloads during autonomous aerial grasping [38]. Grasping non-static payloads enhances the applicability of our SAV, enabling it to contribute effectively to tasks such as drink delivery or environmental cleaning.
- The proposed lightweight soft gripper, coupled with a traditional quadrotor weighing 1002 g, successfully grasps a plastic box weighing 279 g while in mid-air [38]. Furthermore, we demonstrate aerial grasping of a 159 g spherical container. The payload-to-weight ratio achieved by our SAV surpasses those observed in previous investigations on soft grasping [4, 7, 8, 32]. Table 1.1 shows the payload-to-weight ratio of the proposed SAV with the soft gripper consisting of inextensible layers and previous investigations. Note that the weights of all the UAVs in Table 1.1 exclude the weights of their vision-based system.

1.4 Outline of the Thesis

This thesis contains six chapters. This chapter describes the introduction of the thesis.

Table 1.1: Payload-to-weight ratio of the proposed SAV with the soft gripper consists of inextensible layers and the previous investigations.

Proposed SAV [38]	Ping et al. [7]	Sarkar et al. [8]	Cheung et al. [32]	Ubellacker et al. [4]
0.16/1.002 = 0.160	0.13/1.615 = 0.080	0.15/3.684 = 0.041	0.075/0.808 = 0.093	0.148/1.886 = 0.078

The application of aerial grasping is introduced along with safety and efficiency concerns. This is followed by the thesis' three motivations, such as enhancing grasping by using a soft gripper design, simplifying the landing mechanism, and solving the challenges during drone delivery due to the change in the dynamics of the Unmanned aerial vehicle (UAV)s by Disturbance observer-based nonlinear model predictive control (DOMPC). At last, the critical contributions of this thesis are discussed. The following chapters of this thesis are organized as below:

- **Chapter 2** summarized the design and control methods of the soft grippers, including tendon-actuated soft grippers and pneumatic soft grippers, respectively. Comparisons between these two types of soft grippers were given. The implementations of traditional aerial grasping (which consists of rigid grippers) and soft aerial grasping were also illustrated. The characteristics of the existing aerial system and control were also highlighted.
- **Chapter 3** shows the design and control of the proposed modular pneumatic soft grippers with and without inextensible layers. Its mechanical design, fabrication process, and electronics are provided for the grippers' design. Subsequently, the soft grippers' airflow system and pressure regulation are presented. Two solenoid valves manage the airflow system for inflation and deflation, while a feed-forward P controller regulates an air pump to provide the desired pressure. The grasping capability of the soft grippers was tested in the static grasping test with payloads of different shapes and weights.

- **Chapter 4** demonstrates the novel Soft aerial vehicle (SAV)'s design and control. This unique system design incorporates a conventional UAV with an onboard computer and the proposed soft gripper with inextensible layers. Concerning the dynamic change of the suggested SAV due to the additional mass of the grasped object and environmental uncertainties, the linear acceleration disturbances are defined in the dynamic model of the SAV. Furthermore, disturbance observers that use Extended Kalman filter (EKF) and Three-order robust differentiator (RD3), respectively, are designed to estimate the disturbances. After evaluating the two disturbance observers in a position tracking test, the one that utilized EKF had a better tracking performance and was chosen for integration with SAV's NMPC. Moreover, the position tracking performance of this suggested DOMPC was tested with Nonlinear model predictive control (NMPC) and Proportion-Integration-Differentiation (PID) and performed most effectively. After introducing the finite state machine of the aerial grasping mission, the SAV's payload capability, aerial grasping performance, and soft landing ability are discussed.
- **Chapter 5** gives the conclusions of the thesis. The performance of the proposed soft grippers and the soft aerial grasping are summarised. Future work is also suggested based on the potential of outdoor soft aerial grasping. This soft aerial grasping will be considered for integration with outdoor object detection in more drone applications, such as medical delivery and outdoor harvesting.
- **Chapter 6** provides the experimental videos of the proposed SAV and its modular pneumatic soft gripper, including the static grasping test of the gripper with and without the inextensible layers, payload test with various payloads, soft aerial grasping test, and standard landing and tilt landing of the SAV. Both QR codes and the links to the videos are given.

Chapter 2

Literature Review

This chapter introduces current research on the design and control methods for UAVs' soft grippers and aerial grasping systems, respectively.

2.1 Soft Gripper Applications on Unmanned Aerial Vehicles

2.1.1 Tendon-actuated Soft Gripper Design and Control

Inspiring from biological systems such as birds [41], soft grippers have demonstrated the ability to mitigate contact forces and compensate for grasping inaccuracies, exemplifying the concept of morphological computation, which combines passive mechanical components with explicit control [26]. Hence, the bio-inspired tendon-actuated soft gripper was developed since its bending capability can be controlled easily by driving the tendon [1, 42, 43]. Some new quadrotor designs that use soft tendon-actuated grippers to adapt to different environments are as follows:

Ramon-Soria et al. [2] carried out a soft landing gear for focusing on perching. This

aerial system is capable of perching autonomously on pipes for inspection and maintenance in industrial environments. The soft gripper landing system made the drone robustly attach to the pipe. Nylon strands that cross both tentacles longitudinally operate the gripper. A rib made of Polylactic acid (PLA) had been positioned at the tip of the tentacles to tie the threads, increase rigidity, and disperse the forces. The remaining thread ends were spooled around an additional 3D-printed cylinder. A small servo motor installed into the construction moves this cylinder. To encourage the right mobility, a reinforcement made of PLA was positioned at the base of the limb. The servo motors for each limb were intended to be housed in separate chambers at the base of the landing mechanism described above. The landing system was modular, so it was feasible to swap out the gripper swiftly in the event of failure. The stiffness of the joint had to be considered in order to get a decent grip and have the widest grip range. In the outdoor experiment, this soft gripper closed over the pipe when the distance to the pipe was short enough. Even if the Unmanned aerial vehicle (UAV) was not completely centred and fastened to the pipe during the perching, the soft gripper forced the drone into place. Because of this, Ramon-Soria and his team claimed that the quadrotor can work perfectly in windy situations when the control cannot guarantee precise positioning over the pipe.

Fishman et al. [3,44] invented another soft drone with a soft tendon-actuated gripper for dynamic grasping. A human finger inspired the joint placement of the gripper. Each finger is connected to the quadrotor base and propelled by two opposing tendons. Pulling a tendon causes the finger to contract because it passes through a group of nodes linked to the finger. As the soft gripper was operated in an open loop, the measurement of the gripper's state was eliminated. This soft drone aimed to grasp an object of unknown shape lying over an unknown surface. This meant the system was only provided with the centroid of the object. By neglecting the soft gripper dynamics due to their assumption (the soft gripper was quasi-static, which meant there was an instantaneous relation between rest lengths and gripper configuration), the instantaneous rest length of the soft gripper could

be computed and applied in the open loop.

Ubellacker et al. [4] extended the soft tendon-actuated gripper design from [3,44]. They moulded the soft gripper by using Smooth-On FlexFoam-iT! X [45] instead of silicon rubber [46]. Due to the elasticity of the mesh of the flex-foam, their soft gripper remained closing initially. Unlike most soft grippers, its control method focused on commanding the gripper to be opened instead of closing during the grasping mission. When the winch was tightened, the tendons of each soft finger contracted to compress the outer edge of the finger and force the gripper to be opened. Ubellacker and his team also improved the modularity of the soft fingers by allowing the soft finger to be slotted into the base plate of the soft gripper for fast replacement. They also claimed that their soft gripper had simple manufacturability and high repairability. The tears near the base can be easily repaired by common super glue. Although they mentioned that their soft gripper acts as a cushion system during hard landings and no repairs were required after the drone fell over six feet onto solid surfaces, their soft drone still needed a rack for takeoff to ensure the state of the drone was ready for arming the brushless motors. Therefore, their soft gripper did not function as a standard landing gear but could dampen the impact force during landing.

2.1.2 Pneumatic Soft Gripper Design and Control

Since tendon-actuated soft grippers require more complex fabrication (inserting tubes inside the soft fingers for tendons to pass through them) [47,48], pneumatic soft grippers, which only required a sufficient air chamber for each soft finger to conduct bending, gain the attention in the current soft gripper research area [5]. Moreover, the location of the tendon-actuated gripper is constrained by the position of the driven motor. Nevertheless, soft pneumatic grippers offer great configurational flexibility due to the flexibility of the air tube. The air tube can quickly connect the pneumatic soft gripper with the pumps

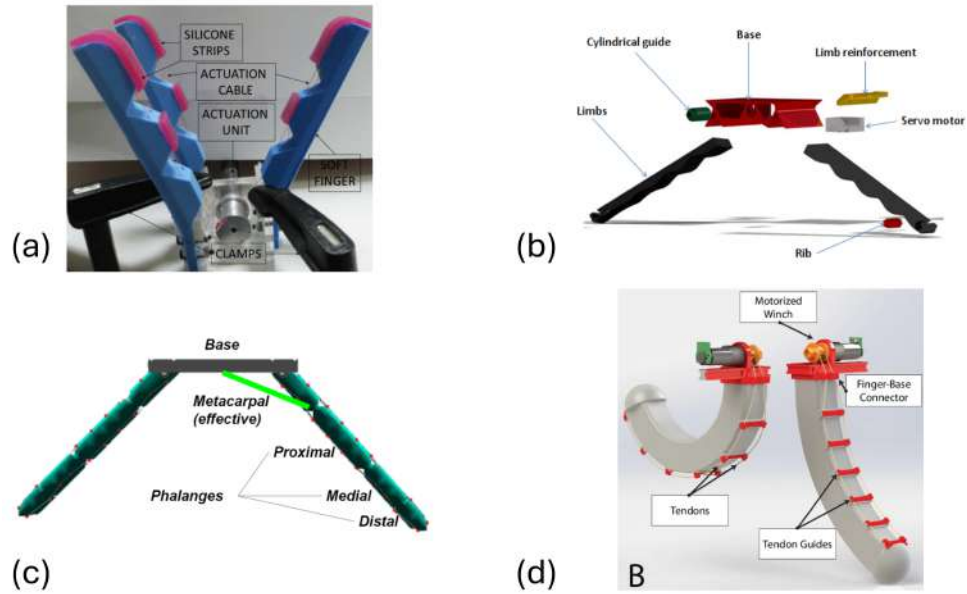


Figure 2.1: Images with (a) a bio-inspired tendon-actuated soft gripper [1], (b) a tendon-actuated soft landing gear [2], (c) a soft tendon-actuated gripper for dynamic grasping [3], and (d) a modular soft tendon-actuated gripper [4].

and valves. However, the common industrial pneumatic system of the soft gripper is too bulky and heavy [49, 50], thereby only a lightweight pneumatic system can be applied on the UAV platform to minimize the effect of the thrust propulsion.

Shtarbanov [6] invented a wearable and modular pneumatic platform, FlowIO, for soft robotics, which showed that the pneumatic system can be a miniature development. The core characteristics of FlowIO are modularity and reconfigurability. Users can quickly configure and reconfigure a FlowIO system to meet their project's pressure, flow rate, and size requirements by exchanging magnetically attached modules thanks to integrated modules with numerous pneumatic configurations. An interconnected main module and pump module make up a complete FlowIO device. The hardware modules enabled a wide variety of pneumatic applications with pressure ranges from -26 psi (-179kPa) to +30 psi (+209 kPa). Although the details of the pressure control of FlowIO were not mentioned, this project proved the potential development of the lightweight and compacted pneumatic gripper system, which is capable of implementing in UAVs' cost-effective aerial grasping.

Two examples of the pneumatic soft gripper applications of aerial grasping are described as follows.

Ping et al. [7] attached a soft pneumatic gripper under a conventional quadrotor, similar to this thesis' idea. Nevertheless, their focus does not explicitly revolve around autonomous aerial grasping tasks or alleviating the need for additional rigid landing gear. The soft gripper was operated by a single control command, which is the pneumatic pressure. This work compared three conditions: the quadrotor alone, with its gripper attached, and various grasped payloads. Ping and his team suggested that the quadrotor (with simple Proportion-Integration-Differentiation (PID) control) may successfully grasp and hold things without dropping them while preserving its dynamics. They stated that the dynamics of the quadrotor were little impacted by the installation of the entire Grasping Unit. Although the simulation behaviour and the real-world flight test behaviour were generally similar in this project, the differences in the altitudes could be more than 0.5 m. This showed that the position control of the experimental flight was not as precise as some current soft aerial grasping research [3, 4].

A two Degrees of freedom (DOF) robot arm with a pneumatic soft gripper was installed under a traditional UAV with the rigid landing gear in [8]. The pneumatic soft gripper utilized semi-circular polymer rings and inextensible layers (made of cotton fabric) to reinforce the stiffness of the soft gripper. Sarkar et al. [8] only controlled the inflation of the soft gripper by pressure regulation to conduct grasping. A single pneumatic battery, which was a plastic air tank with pressurized air, supplied the required air pressure to the soft gripper's air chambers. The gripper control system involved a pressure sensor and two solenoid valves. Following the feedback from the pressure sensor by a microcontroller, the valves managed the airflow direction. Regardless of the soft gripper's lack of a deflation function to enlarge the grasping tolerance, Sarker and his team presented that the gripper could grab a maximum size of around 120 mm. Besides, they stated that the target capability of the payload was 500 g, while a successful grasping of an 814 g payload was

tested.

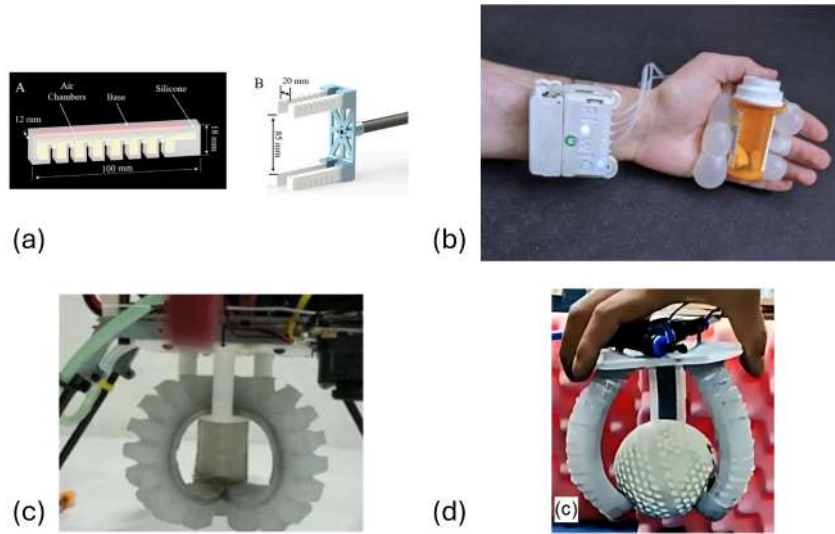


Figure 2.2: Images with (a) a pneumatic soft gripper with inextensible layers [5], (b) a lightweight wearable pneumatic gripper [6], (c) a three-finger pneumatic soft gripper [7], and (d) a pneumatic soft gripper with inextensible layers and semi-circular polymer rings [8].

2.1.3 Comparison of Tendon-actuated Soft Grippers and Pneumatic Soft Grippers

Based on the above-existing research on soft gripper design and control, Table 2.1 summarized the differences between tendon-actuated soft grippers and pneumatic soft grippers. Compared to the tendon-actuated soft gripper, the main advantage of the pneumatic soft gripper is that it changes its configuration more easily, which can offer higher flexibility for target objects with various shapes and dimensions. Therefore, the pneumatic soft gripper is chosen in this thesis.

Table 2.1: Comparison of tendon-actuated soft gripper and pneumatic soft gripper.

	Tendon-actuated	Pneumatic
Actuators	Servo motors/DC motors and tendons	Air pumps and solenoid valves
Control method	Pulling tendons	Pressure regulation and airflow control
Fabrication	Inserting tubes in the soft fingers' body for tendons installation	Leaving air chambers inside the soft fingers by moulding
Configuration changes	Harder (limited by the position of the motors)	Easier (benefited by the flexibility of the air tubes)

2.2 Aerial Grasping System and Control

2.2.1 Rigid Aerial Grasping System and Control

Aerial grasping is a popular research area, especially for those using rigid grippers. [9, 51] proposed a quadrotor control system for aerial grasping and harvesting with a rigid gripper, where they suggested fusing Inital measurement unit (IMU) data using an Extended Kalman filter (EKF) to provide acceleration feedback. As the drone was designed for fruit harvesting, Kumar and Behera [9, 51] placed the rigid gripper with a three-finger hand jaw in the forehead of the drone instead of the drone's bottom to grasp the fruits horizontally. To conduct indoor and outdoor harvesting, the drone provided indoor and outdoor fruit detection through learning-based object detection by a commercial dual camera. The above visual perception demonstrated GPS-denied autonomous aerial grasping of the apples.

A biomimetic Unmanned aerial vehicle (UAV) designed by Roderick, Cutkosky, and Lentink [10] is inspired by birds that can dynamically perch on complicated surfaces and grasp irregular targets with their two legs. This rigid gripper replaced the traditional

rigid landing gear and allowed the UAV to do perching in forest environments. The mechanism design of the gripper was bio-inspired by birds' hindlimbs, which was much more complicated than other commercial rigid grippers. The perching ability of this UAV in a forest was tested by the pilot who flew the UAV manually with a remote controller. The proposed gripper can also catch some objects with similar sizes and weights. The objects were hand-launched at the vehicle. This research mainly focused on autonomous rigid gripper control for successful perching and grasping.

Thomas et al. [11] proposed an ordinary UAV with a rigid under-actuated gripper to conduct dynamic grasping of a suspended object. This aimed to avoid unplanned contact forces. The grasping was conducted by using vision feedback from a monocular camera and an IMU onboard the UAV. An Image-Based Visual Servoing (IBVS), which directly uses feedback from the image coordinates, was developed based on the visual features of a cylinder (target objects). Hence, this research did not require an external motion capture system for trajectory tracking.

A rigid aerial grasping of a morphing UAV was developed. Bucki, Tang, and Mueller [12] suggested a novel quadcopter with unactuated hinges to perform grasping by landing on the targets (see also [52]) but also focused on traversing small passages and perching on hanging wires. A cascaded controller was used to control the hover of this vehicle because of its simplicity and popularity. Also, different infinite-horizon LQR controllers were synthesized to control the vehicle's attitude when flying in different configurations. To save computational power and reduce the complicity of the drone's hardware design, Bucki and his teammates chose to use an LQR controller, which is straightforward and can be run on low-power embedded devices with little setup. However, the grasping performance of this novel vehicle was not as good as its traverse. These unactuated hinges required over 10 seconds to hover over the targets for their aerial grasping tasks. Moreover, only rectangular objects with the specific dimension (referring to the UAV airframe) could be grasped as the UAV had to land on the object and deform its four hinges to do grasping.

These minimal grasping capabilities were demonstrated and admitted.

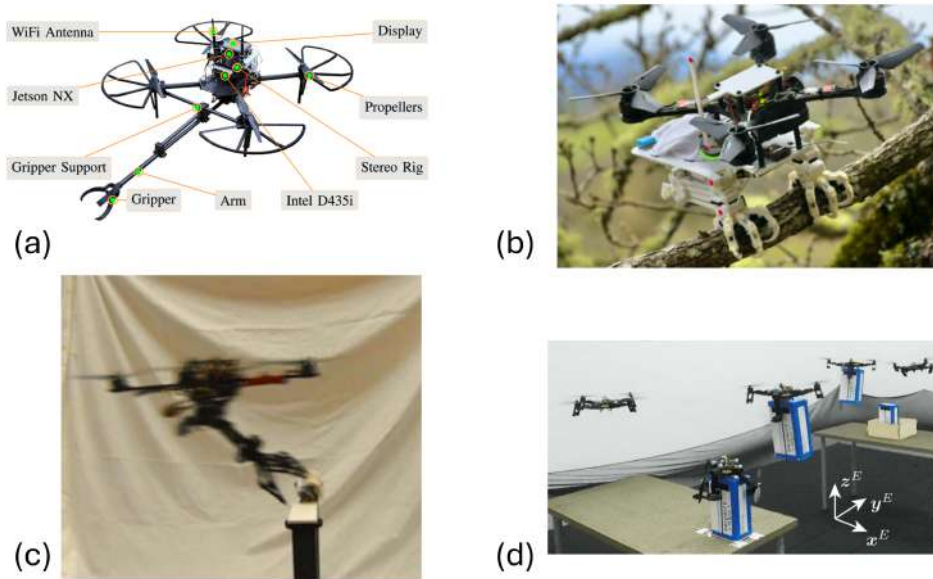


Figure 2.3: Images with (a) an aerial harvesting system by a rigid gripper [9], (b) a perching system by a rigid gripper [10], (c) aerial grasping of a suspending object with a rigid gripper [11], and (d) rigid aerial grasping by unactuated hinges of a quadrotor [12].

2.2.2 Soft Aerial Grasping System and Control

On the other hand, more soft aerial grasping systems were developed due to increased investigations into soft grippers. Some Soft aerial vehicle (SAV) need to hover over the target object before grasping or perching [53–55]. More examples of soft aerial grasping systems are introduced below.

Fishman et al. [3, 56, 57] developed a soft drone with a soft gripper (also as the landing gear) to conduct dynamic grasping. The soft drone grasping performance was first evaluated by simulation [44], and then a real-world experiment was conducted in a motion capture room. Their approach eliminates the need to measure the gripper state. However, they operate the soft gripper in an open-loop manner to grasp objects with unknown shapes on unknown surfaces, relying on the centroid of the objects. But it only tried to

grasp a table-like foam target in the motion-capture room. An adaptive geometric controller controlled the proposed soft drone, and a minimum-snap trajectory optimizer did its trajectory planning [58]. Their suggested controller aimed to compensate for disturbances caused by the target object and unmodeled aerodynamic effects during dynamic grasping. Although the proposed dynamic grasping provided a smooth grasping trajectory, the grasp speed of the soft drone is 0.2 m/s, which is a relatively slow speed in aerial manipulation. In [56], robust or adaptive Nonlinear model predictive control (NMPC) was suggested for the soft drone to grasp moving targets. Linear Model predictive control (MPC) was not recommended as this significantly restricts the quadrotor's ability to track moving targets while performing abrasive manoeuvres.

Building upon [3], Ubellacker et al. [4,59] presented another approach for aerial grasping with onboard perception using a soft drone. Their adaptive controller only considered external disturbances for translational dynamics instead of rotational dynamics. They also added a feed-forward acceleration impulse to compensate for the z-direction disturbance induced immediately after grasping an object. The target localization provided by their perception system design also demonstrated aerial grasping of moving objects.

Some existing works focus on UAV control for soft aerial perching or grasping with static payloads. Ramon et al. [2] designed a soft landing gear system that enables autonomous perching of a drone on pipes for inspection and maintenance. They use a neural network to estimate the position, filtered by an EKF and used as a reference for the control loop. A Proportion-Integration-Differentiation (PID) controller generates speed commands for the flight controller to regulate the drone's location. The visual estimation is also utilized for controlling the orientation of the drone.

Ping et al. [7] integrate a soft pneumatic gripper beneath a conventional drone, similar to our design. Their soft drone utilizes a PID controller within the Flight control unit (FCU). However, their primary focus does not revolve explicitly around autonomous aerial grasping tasks or alleviating the need for additional rigid landing gear. The lack

of additional Degrees of freedom (DOF) in their gripper design, which could facilitate grasping, limits the grasping altitude of the drone due to the presence of rigid landing gear. They claim that their soft gripper has minimal impact on the dynamics of the drone and tested its hovering ability with various payloads weighing up to 100 g.

In the work of [8], a robot arm with a pneumatic soft gripper was developed under a conventional drone. Hence, extra mechanisms and control algorithms were needed to ensure the aerial grasping system’s manipulator could reach its home and pick positions. The control of this drone relies on the Ardupilot Firmware and QGroundControl station. Sarkar et al. [8] mentioned an outdoor packet delivery test was conducted successfully. The packet weighed approximately 150 g, while their quadrotor with soft gripper weighed over 3.5 kg. Although the details of the position tracking performance of the outdoor aerial delivery task were not given, the total time of flight and target hovering altitude were provided to evaluate the efficiency.

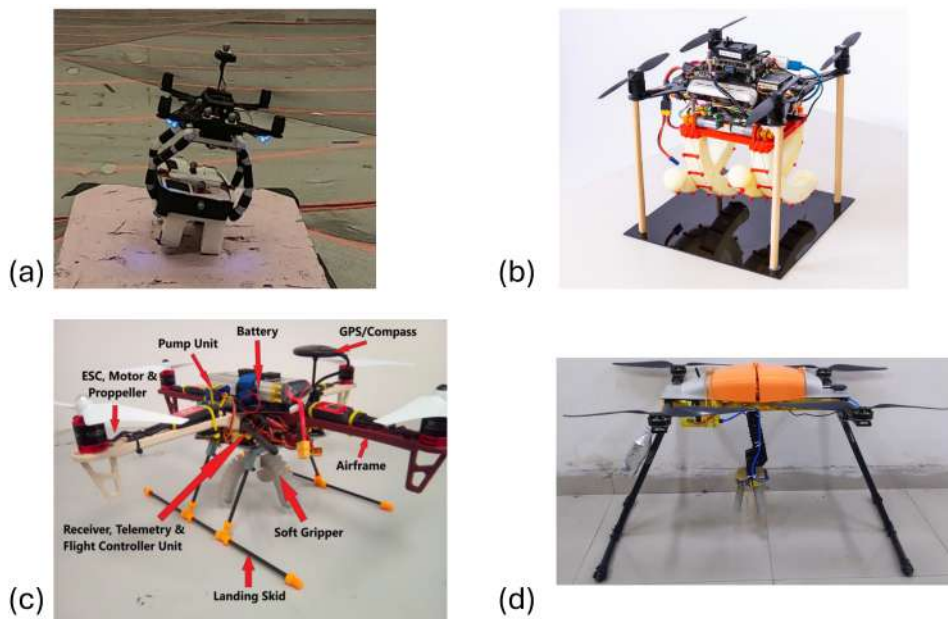


Figure 2.4: Images with (a) dynamic grasping [3], (b) a soft drone with onboard perception [4], (c) soft drone with a pneumatic gripper and a rigid landing gear [7], and (d) soft drone with a robot arm that contains a soft pneumatic gripper [8].

2.2.3 Comparison of Aerial Grasping with Soft Gripper and Rigid Gripper

Based on the above-existing research on aerial grasping system and control, Table 2.2 summarized the comparison of aerial grasping with soft gripper and rigid gripper. Compared to aerial grasping with a rigid gripper, the main advantage of aerial grasping with a soft gripper is that it can grasp the target objects with less impact force, consist simpler mechanism, be fabricated more easily by moulding without complicated structure and extra fasteners, and provide a lightweight characteristics of the system by eliminating robot arm. Therefore, the aerial grasping system with a soft gripper is suggested in this thesis.

Table 2.2: Comparison of aerial grasping with soft gripper and rigid gripper.

	With Soft Gripper	With Rigid Gripper
Impact force to target	Lower	Higher
Mechanism	Less complicated	More complicated
Fabrication	Easier (moulding)	Harder (requires more components)
Robot arm	Not necessary	Usually requires

Chapter 3

Modular Soft Gripper Design and Control

3.1 Mechanical Design

The proposed soft grippers have two configurations: an X-base and an H-base. Both X-base and H-base configurations require four soft fingers to grasp the target objects, as four soft fingers can provide a larger pinching force than three or fewer soft fingers. [7,60]. Each soft finger consists of one air chamber. The four air chambers of the soft gripper are interconnected and equipped with one micro-pump and two solenoid valves. The details of the electronics parts will be mentioned in Section 3.3. Inflation and deflation of the soft fingers can be conducted by the airflow direction (controlled by valves) and the micro-pumps (providing pumping and vacuuming simultaneously). The pressure regulation of the soft gripper is presented in Section 3.4. The modular connectors of the soft fingers have been designed to simplify the attachment of the soft fingers to various bases. Sliding the connector and securing it with a screw allows each soft finger to connect to different bases to grasp different objects quickly. This approach reduces the required number of soft fingers to a maximum of four, significantly reducing assembly time.

3.1.1 Structure of Pneumatic Soft Gripper Without Inextensible Layers

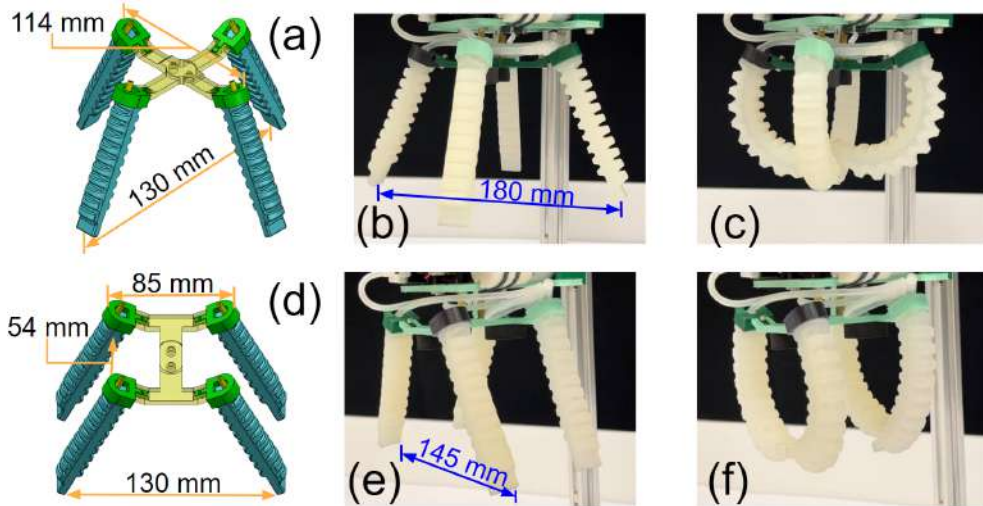


Figure 3.1: Dimensions of the X-base (spherical) soft gripper when it is (a) initially opened, (b) fully opened, and (c) fully closed. And the dimensions of the H-base (cylindrical) soft gripper when it is (d) initially opened, (e) fully opened, and (f) fully closed.

These soft fingers are 100 mm long and 15 mm wide. They are affixed to the two bases at a 25° inclination angle, giving the gripper increased grasping tolerance and diverse options for target objects. Grasping tolerance refers to the available dimension for grasping when the gripper is deflated, precisely the distance between the fingertips when the gripper is fully opened in Fig. 3.1(b) and Fig. 3.1(e), respectively. The diagonal distance of the fully opened X-base (spherical) soft gripper is 180 mm, while the tip-to-tip distance of the fully opened H-base (cylindrical) soft gripper is 145 mm. The dimensions of the two bases are shown in Fig. 3.1(a) and Fig. 3.1(d). When the complete closing of the soft gripper is undergoing, all tips of the soft fingers of the X-base soft gripper touch each other, while the tips of the two pairs of the 2-tip soft fingers of the H-base counterpart touch each other too (see Fig. 3.1(c) and Fig. 3.1(f)). The weights of the H-base and X-base soft grippers are 106 g and 110 g (excluding the electronics), respectively.

3.1.2 Structure of Pneumatic Soft Gripper With Inextensible Layers

To enhance the pinching force of the soft gripper, we improve their mechanical structure by adding an inextensible layer to each of them. These soft fingers have dimensions of 90 mm in length and 20 mm in width. These soft fingers with the inextensible layers are shorter than the previous design because of their higher stiffness. Hence, to keep using the same electronics and control system, these fingers need to be shorter to maintain their bending ability to grasp. Moreover, their wall thickness is also higher than the previous design to avoid the risk of air leakage under a long inflation time. These fingers are also attached to the two bases at an inclination angle of 25° . The grasping tolerance for the H-base soft gripper is $150 \times 90 \text{ mm}^2$, while the x-base soft gripper has a grasping tolerance of 160 mm diagonal distance. The details of the dimension of the soft gripper when it is initially opened, fully opened and fully closed are illustrated in Fig.3.2. The weights of the H-base and X-base soft grippers are both 124 g (excluding the electronics).

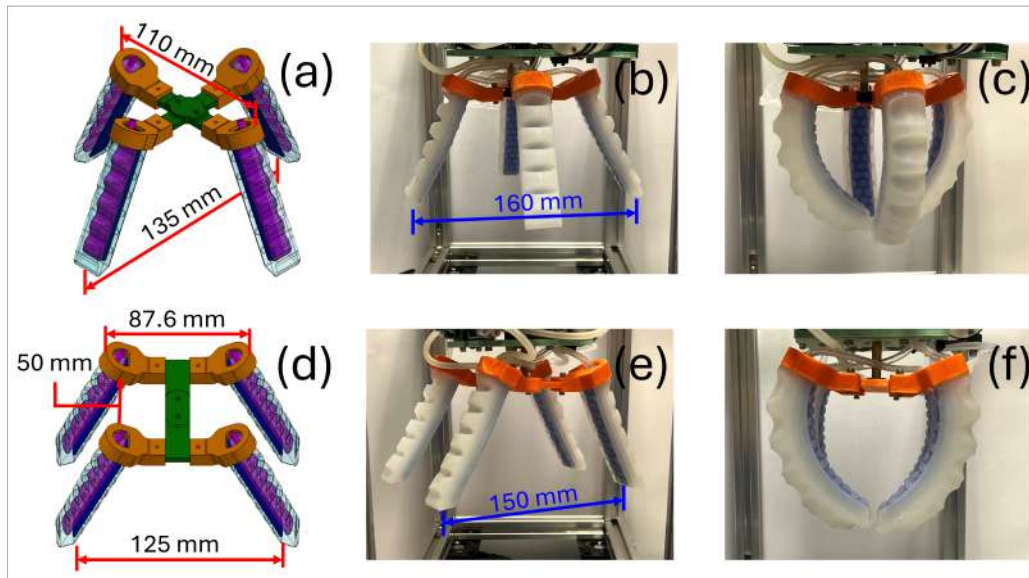


Figure 3.2: Dimensions of the X-base (spherical) soft gripper when it is (a) initially opened, (b) fully opened, and (c) fully closed. And the dimensions of the H-base (cylindrical) soft gripper when it is (d) initially opened, (e) fully opened, and (f) fully closed.

3.2 Fabrication

The proposed soft gripper is made of silicone rubber (*Smooth-On Dragon Skin 30*) with 30 A shore hardness [46], while all moulds, connector of each soft finger, and the two bases are made of Polylactic acid (PLA) by 3D printing [61]. All moulds of the two soft grippers can be downloaded via this link: https://github.com/Athenachc/sav_gripper. Details of the manufacturing process of the two soft gripper designs are shown in the following subsections.

3.2.1 Details of Pneumatic Soft Gripper Without Inextensible Layers

Fig. 3.3 illustrates the moulds of a pneumatic soft finger that is described in Section 3.1.1. There are two parts to the moulds: one makes the main body of the soft finger with its air chamber, while another produces the cover of the soft finger.

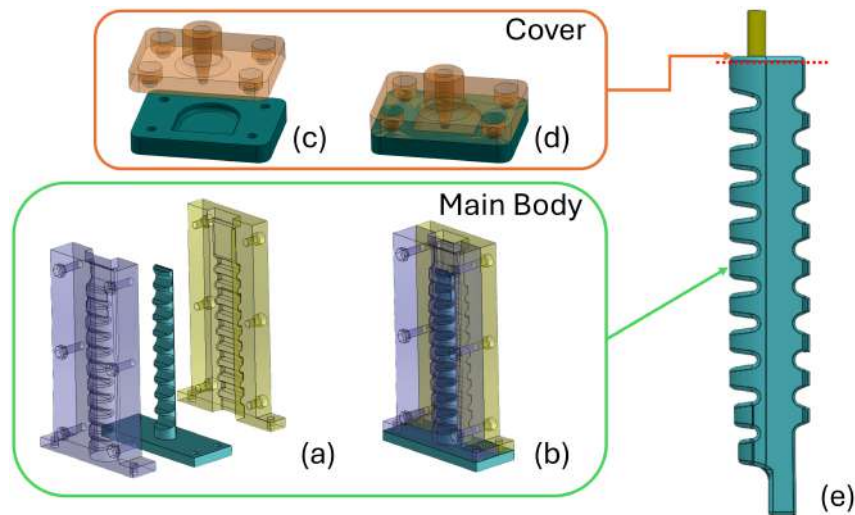


Figure 3.3: The exploded view (a) and assembly (b) of the mould of the soft finger's main body. The exploded view (c) and assembly (d) of the mould of the soft finger's cover. (e) The side view of the soft gripper.

Referring to [62], the details of the fabrication process of a soft finger are described as follows. First, spray the resin mould release to the mould, which is depicted in the middle of Fig. 3.3(a), wrapped in liquid silicone rubber to make an air chamber in the main body. Hence, this mould can be removed easily after curing. Then, assemble the moulds for the main body and cover the soft finger. Next, pour the liquid silicone rubber into the moulds for the main body and cover separately. After the silicone rubber finishes curing inside the moulds, a small hole is cut on each finger's cover. This allows the silicone tube to pass through the cover and be fixed by adhering it with resin glue. Then, the main body and the cover with the silicone tube can be glued with resin glue, too.

Notably, only the mould used to make the air chamber is disposable since it will be twisted and bent during removal from the soft finger. Nevertheless, the rest of the moulds can be reused to save future fabrication time.

3.2.2 Details of Pneumatic Soft Gripper With Inextensible Layers)

Compared with the above design, an inextensible layer made of Thermoplastic polyurethane (TPU) with a shore hardness of 80 A is placed inside the back of each soft finger (next to its air chamber) to enhance the pinching force [63,64]. This inextensible layer is also fabricated by 3D printing.

The manufacturing process of this soft finger with the inextensible layer is similar to the above method (Section 3.2.1). Additional steps are adhering TPU on the back of the soft gripper and then adhering them with the main body and the cover of the soft gripper. Fig. 3.4 describes moulds for fabricating the three parts of the soft finger with an inextensible layer. Besides, adhering moulds are used to quickly align the three parts of the soft finger (see Fig. 3.5).

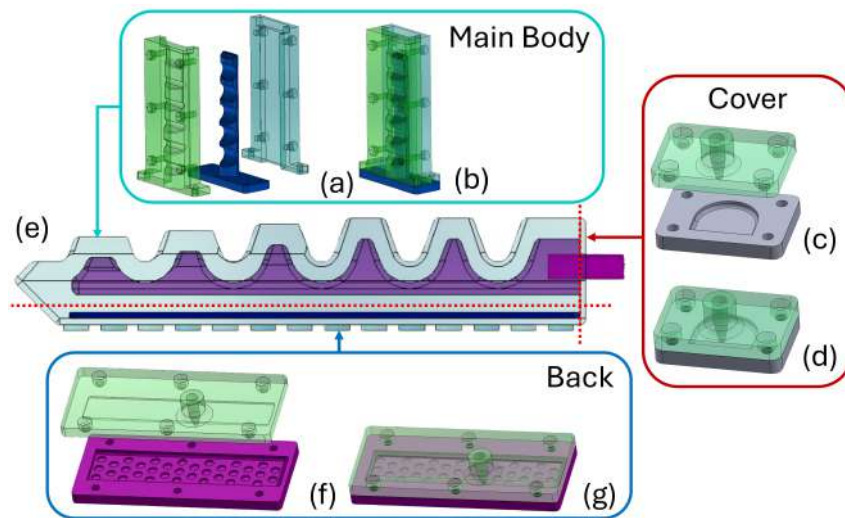


Figure 3.4: The exploded view (a) and assembly (b) of the mould of the soft finger's main body. The exploded view (c) and assembly (d) of the mould of the soft finger's cover. (e) The side view of a soft gripper. The exploded view (f) and assembly (g) of the mould of the back of the soft finger.

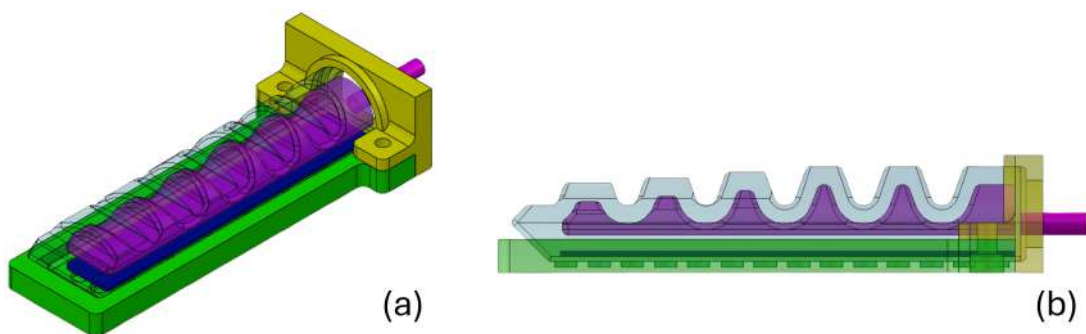


Figure 3.5: Moulds for adhering the soft finger with an inextensible layer: (a) isometric view and (b) side view.

3.3 Electronics

The main electronic components of the proposed soft gripper system are an ESP32-S3 microcontroller, an air pump, and two solenoid valves. A Pulse-width modulation (PWM) signal from the flight controller is sent to the microcontroller for airflow control and pressure regulation (see Fig. 4.15). Note that the microcontroller passes another PWM signal for pump inflation or vacuum during pressure regulation. As the air pump facilitates both inflation and deflation simultaneously, two solenoid valves are required to serve as switches to control the airflow. Details of the airflow control are mentioned in Section 3.4.1. The pressure range of the air pump is $[-60, 120]$ kPa, while the pressure sensor with a range of $[-100, 300]$ kPa is used to detect the airflow pressure within the air chambers of the gripper and provide feedback to the microcontroller. To reduce the electronics' weight and the electronic connections' complexity, a customized Printed circuit board (PCB) integrates the microcontroller, pressure sensor and the necessary resistance and capacities (except the air pump and the two air valves). During our experiment trials, the commercial thin-film force sensor was not sensitive enough to detect the gripper force. Thus, we only checked the grasp status with our bare eyes and excluded the force sensor of the gripper system. The total weight of the electronic components is 146 g [32]. Fig. 3.6 illustrates the electronic components of the soft gripper with their weight information.

The payload capacity and the efficiency of the Soft aerial vehicle (SAV) are the main concerns during the design process of the soft gripper. Thus, the selected air pump and solenoid valves are lightweight to save the maximum load of the SAV. In Fig. 3.6, an air pump and a solenoid valve weigh 61 g and 15 g, respectively. Also, to further reduce the weight of the SAV, the soft gripper does not need an extra power source when installed under a traditional quadrotor. This minimizes energy requirements, enabling the soft gripper to operate efficiently with the existing quadrotor power system. Hence, the payload capacity of the SAV can be maximized [32].

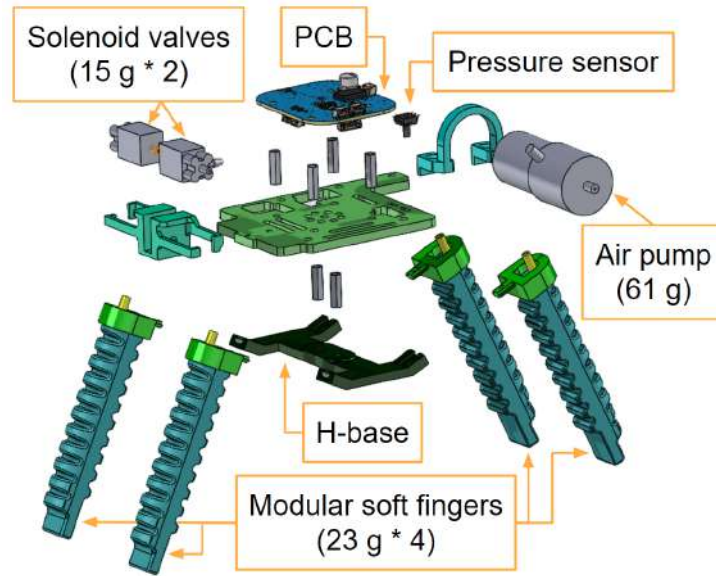


Figure 3.6: The exploded view of the electronics of the soft gripper with weight information.

3.4 Control of Soft Gripper

The control of the proposed pneumatic soft gripper includes its airflow control system and pressure regulation. Before grasping, the desired pressures for inflation and deflation of the soft gripper have to be set to the ESP32-S3 microcontroller.

3.4.1 Airflow Control System

The deflation process allows the soft gripper to open, release, and land, while the inflation process activates the grasping of the gripper by complete closing. When the soft drone takes off and starts approaching the target object, a command of deflation, which is an input Pulse-width modulation (PWM) signal, is sent to the flight controller by the ground control station [32] or an onboard computer. This command activates the deflation airflow through the solenoid valves and initiates vacuuming with the air pump. Then, the flight controller passes the PWM input of deflation to the soft gripper microcontroller. Hence,

the air pump starts vacuuming by a feed-forward proportional controller (see Fig. 3.8), so the soft gripper is “opened” by deflation. The soft gripper keeps deflating until the flight controller receives the inflation command and triggers the soft gripper to close. Similarly, the inflation also passes from the ground control station [32] or an onboard computer to the microcontroller of the soft gripper. This makes the gripper "closed" and grasps the target object.

There are three ranges of the PWM inputs to the microcontroller for staying at rest, inflation, and deflation. The airflow of the system during inflation and deflation are shown in Fig. 3.7a and Fig. 3.7b, respectively. Only the relevant valve is activated during inflation or deflation, while the other valve remains off to ensure correct airflow direction. In Fig. 3.7, the blue solid block and the red solid block of the air pump represent the inflation and deflation function of the pump mainly used in the relevant airflow, respectively. Also, the blue and the red lines and arrows indicate the inflation and the deflation airflow of the gripper, respectively.

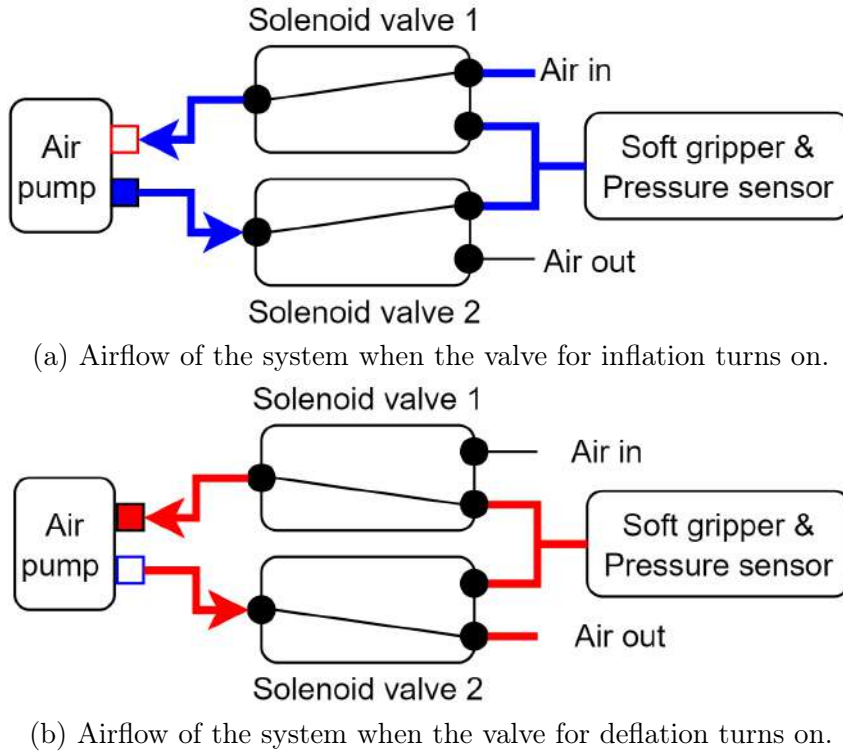


Figure 3.7: Airflow of the soft gripper’s system.

3.4.2 Air pump Regulation

The pressure regulation of the soft gripper is conducted by feed-forward proportional control, which combines feed-forward and proportional control techniques to enhance performance by anticipating the impact of input pressure changes on output pressure. In a typical proportional control, pressure feedback is received by the pressure sensor so the proportional control can adjust the pressure output accordingly. However, in this feed-forward proportional control, the feed-forward component can anticipate the effect of changes in the input pressure on the output pressure. Due to the limited performance of the lightweight air pump and the unseal soft gripper system, which enables easy swapping between two configurations, slight air leakage can be predicted as a disturbance of the pressure regulation [32]. Therefore, by integrating the feed-forward and proportional control strategies, the gripper achieves faster response times and improved stability in regulating the air pump. Fig. 3.8 shows the block diagram of the feed-forward proportional controller for the air pump regulation of the proposed soft gripper.

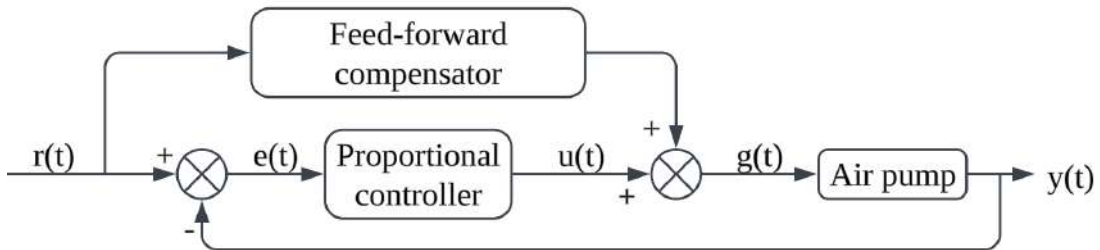


Figure 3.8: Block diagram of feed-forward proportional control of the soft gripper.

Notably, the feed-forward proportional control only sets the PWM signal for the air pump. At the same time, the PWM command of the flight controller directly determines the digital signals for activating the valves. This valve control strategy prevents excessive vibration caused by rapid changes in airflow direction. Only the PWM signal of the air pump is set by the feed-forward proportional controller. Simultaneously, the digital signals of the solenoid valves are desired by the PWM command of the flight controller

directly. This valve control strategy can prevent excessive vibration of the soft gripper due to rapid changes in the airflow direction.

The feed-forward proportional controller in Fig. 3.8 can be computed by solving the following equations [32]:

$$e(t) = r(t) - y(t) \quad (3.1)$$

$$u(t) = K_p \times e(t) + p_{min} \quad (3.2)$$

$$K_p = \frac{p_{max} - p_{min}}{r(t)} \quad (3.3)$$

$$g(t) = \begin{cases} u(t) + f_{in} \times y(t) & \text{if inflation} \\ u(t) + f_{de} \times y(t) & \text{if deflation} \end{cases} \quad (3.4)$$

where the minimum PWM duty cycle of the air pump, p_{min} , is an adjustable parameter to optimize the performance according to the desired pressure. If p_{min} is too low, the response time of the system will be longer. The maximum PWM duty cycle of the air pump, p_{max} , is fixed at the 8-bit capacity of the microcontroller of the gripper. Referring to the experimental results, the optimal feed-forward component for inflation, f_{in} , and deflation f_{de} can be observed to speed up the inflation and deflation time of the soft gripper. Further details and explanations of the abovementioned variables can be found in Table 3.1.

Pressure Regulation of Pneumatic Soft Gripper Without Inextensible Layers

The soft gripper focuses on achieving maximum openness and a secure grasp by pressure regulation. After considering factors such as the air chamber capacity, inflation time, performance of the lightweight air pump, and the results of the feed-forward proportional controller, an inflation pressure of 85 kPa is optimal for achieving the desired level of openness. Also, a deflation pressure of -25 kPa is chosen to ensure rapid and effective

Table 3.1: Parameters in air pump regulation.

Variables	Definitions
$e(t)$	Pressure error in kPa
$r(t)$	Set (desired) pressure
$y(t)$	Current pressure
$u(t)$	Output by Proportional controller
Kp	Proportional gain
p_{max}	Max. PWM duty cycle of air pump (100%)
p_{min}	Min. PWM duty cycle of air pump
f_{in}	Feed-forward component for inflation
f_{de}	Feed-forward component for deflation
$g(t)$	Output by Feed-forward proportional controller

closure. The observed optimal p_{min} , f_{in} , and f_{de} are presented as follows:

$$p_{min} = \begin{cases} 86\% & \text{if inflation} \\ 63\% & \text{if deflation} \end{cases} \quad (3.5)$$

$$\begin{aligned} f_{in} &= 0.8 \\ f_{de} &= \frac{1}{r(t)} \end{aligned} \quad (3.6)$$

The step response graph in Fig. 3.9 illustrates the pressure regulation performance with a set pressure signal (set pressure in 0 kPa, -25 kPa, and +85 kPa) by the feed-forward proportional controller and the proportional controller. Although the deflation performance for both controllers is similar, the inflation time of the feed-forward proportional controller is much faster than that of the proportional controller. These results show that the feed-forward component anticipates set pressure changes, facilitating stable current pressure and reduced steady-state error. Also, in the feed-forward proportional control, the desired inflation pressure can be reached faster than the proportional control. Still, the desired deflation performance of both control methods differs insignificantly.

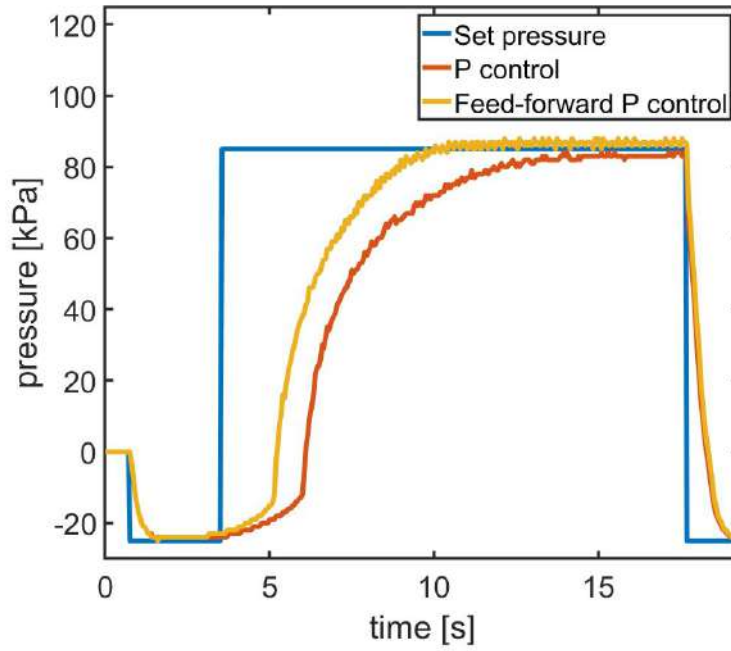


Figure 3.9: Comparison between feed-forward proportional controller and proportional controller of the soft gripper.

Note that the soft gripper starts closing at 58 kPa and takes approximately 5 seconds to reach the proposed inflation pressure from deflation.

Pressure Regulation of Pneumatic Soft Gripper With Inextensible Layer

After considering the increased stiffness of this soft gripper with an inextensible layer, the magnitudes of both desired inflation and deflation pressure have risen. An inflation pressure of 90 kPa is optimal for achieving the desired level of openness, while a deflation pressure of -30 kPa is chosen to ensure rapid and effective closure. The soft gripper starts closing at 60 kPa and also takes approximately 5 seconds to reach the proposed inflation pressure from deflation. Compared to the previous case, only f_{de} remains unchanged in this case. The updated p_{min} and f_{in} are shown as follows:

$$p_{min} = \begin{cases} 73\% & \text{if inflation} \\ 61\% & \text{if deflation} \end{cases} \quad (3.7)$$

$$f_{in} = 2 \tag{3.8}$$

3.5 Static Grasping Test

To further evaluate the grasping performance of the Soft aerial vehicle (SAV), a static grasping test aimed to assess both the maximum load capacity of the soft gripper and its ability to grasp objects with various base shapes. The test involved evaluating the performance of the gripper under different load conditions and its ability to grasp objects with diverse base configurations securely.

In this experiment, the SAV was put on an aluminium rack. The servo tester provided the inflation or deflation Pulse-width modulation (PWM) input signal to the microcontroller of the gripper, making it independent of the drone system without receiving inputs from the flight controller or ground control station [32]. Human hands manually placed target objects under the centre of the gripper. To test the grasping tolerance of the gripper, the positions of the centroid of the objects did not require a precise alignment of the centroid of the gripper before grasping. Successful grasping trials required the gripper to hold the target object for at least 30 seconds. Human hands intentionally moved and gently shook the SAV during the test to ensure a reliable grip. A video of this static grasping test for the two types of soft grippers is attached in the Section 6.1.

3.5.1 Results of Pneumatic Soft Gripper Without Inextensible Layers

Referring to [32], ten grasps were conducted for each specimen. The ten objects in the grasping test are shown in Fig. 3.10.



Figure 3.10: Tested Object Set: (a) Pen Holder with Loads, (b) Computer Mouse, (c) Double-sided Tape, (d) Pen, (e) Spray Paint, (f) Syringe, (g) Membership Card, (h) Pocket Tissue Paper, (i) Spherical Container with Loads, (j) Plastic Box.

From Fig. 3.11, the soft gripper with both configurations can grasp the pen holder and the pocket tissue paper with a 100% success rate. The 4-tip soft gripper with an H-base is designed for grasping cylindrical objects and offers increased gripping force through the wrapping motion of its two pairs of 2-tip grippers. The H-base gripper can grasp cylindrical objects up to 200 g with a 100% success rate, but it has an 80% success rate for grasping a can of spray paint due to the non-static centre of gravity. It cannot handle items more miniature than the distance between its finger pairs, so it is less effective with spherical objects. To address these limitations, a proposed X-base allows all four fingers to align with the centroid of objects to grasp spherical items. It can also grasp the pen holder with loads up to 330 g because one of the soft fingers can hang the pen holder with the support of the other three soft fingers. Nonetheless, the X-base does not provide the same wrapping force for cylindrical objects as the H-base. Thus, X-base and H-base serve distinct purposes. Some examples of this static grasping test are illustrated in Fig. 3.12. Note that the pinching force of a 2-tip soft gripper is much less than the above two configurations of the soft gripper [32]. Hence, the 2-tip soft gripper is negligible in this section.

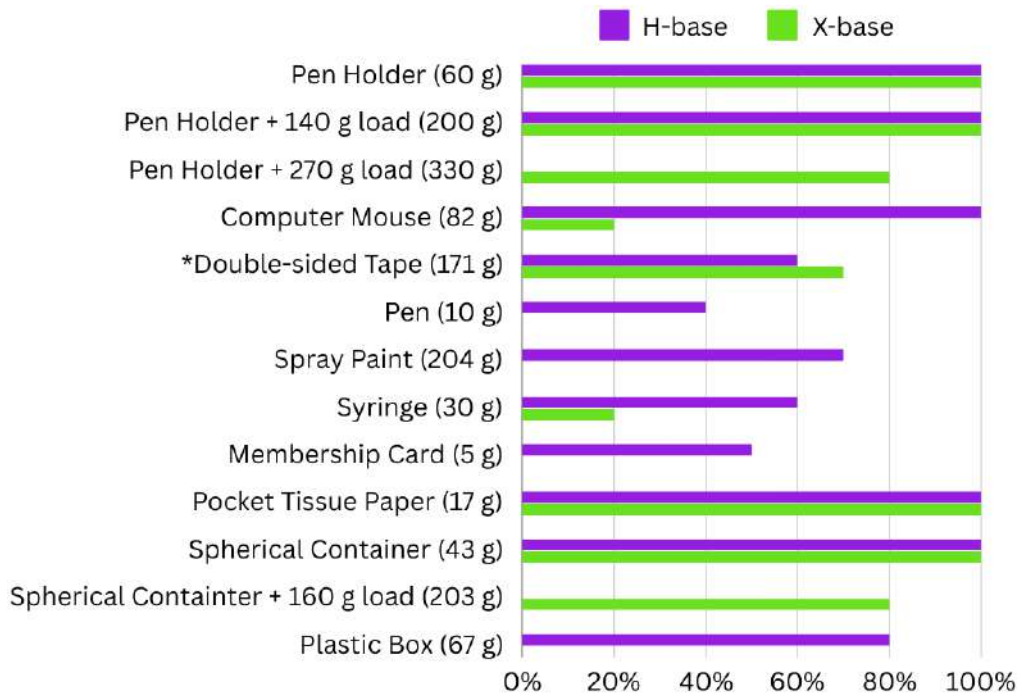


Figure 3.11: Grasping success rate results of 2 configurations.

*The X-base gripper can hang and wrap the tape, while the H-base gripper always wraps the tape.

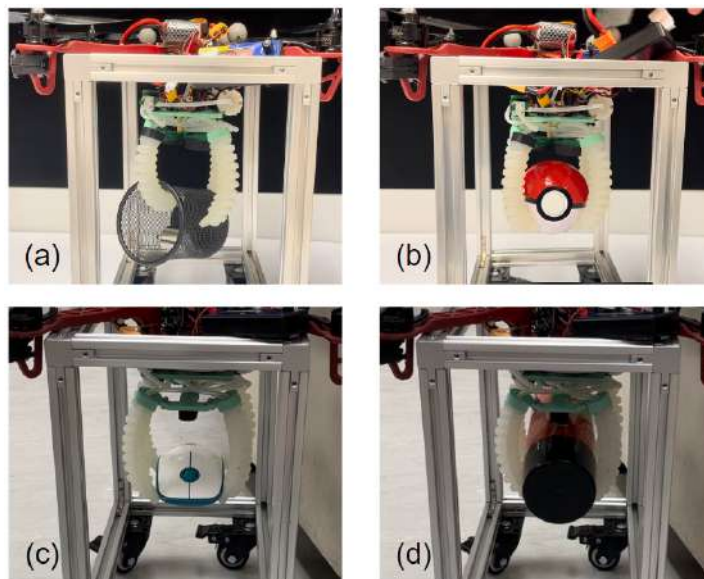


Figure 3.12: Examples of grasping tests: Grasping (a) a pen holder with 270 g loads and (b) a spherical container with 160 g loads by an X-base gripper; Grasping (c) a computer mouse and (d) a can of spray paint with an H-base gripper.

3.5.2 Results of Pneumatic Soft Gripper With Inextensible Layers

Based on the grasping results in Section 3.5.1, the same static grasping test was repeated to determine the maximum load capacity of the soft gripper with an inextensible layer. Fig. 3.13(a) and (b) depicted the grasping of the experimental maximum load of the two configurations of the soft gripper, respectively. The X-base soft gripper with the inextensible layer can grasp a 409 g plastic beaker with three roll rulers, while the H-base soft gripper can grasp a 342 g lead-free circuit board cleaner. Notably, the circuit board cleaner has a non-static mass since it contains liquid.

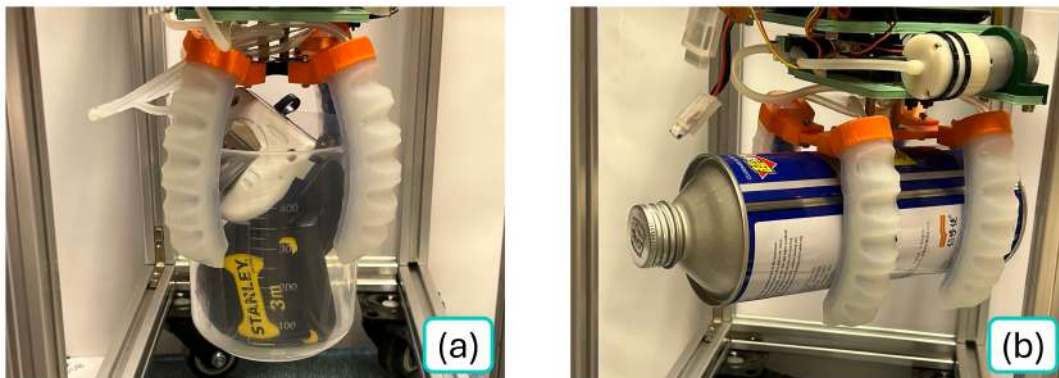


Figure 3.13: Demonstration of grasping (a) a 409 g plastic beaker with three roll rulers by an X-base gripper and (b) a 342 g lead-free circuit board cleaner with an H-base gripper.

We can see the similar grasping performance of the two configurations between the two types of soft grippers. The X-base soft gripper can hold heavier objects because its four soft fingertips can point to the centroid of the round or spherical object together and wrap it. However, the H-base soft gripper separates its grasping force by its two pairs of two-tip soft fingers to grab cylindrical or rectangular target objects. Therefore, the H-base soft gripper has less load capacity than the X-base soft gripper.

3.5.3 Comparison of the Results of the X-base and H-base Soft gripper

Referring to the above static grasping test results, Table 3.2 summarized the comparison between the X-base soft grippers and the H-base soft grippers.

Table 3.2: Comparison of the Results of the X-base and H-base Soft gripper.

X-base Soft Gripper	H-base Soft Gripper
All fingertips point towards the centroid of the objects	Wrap the lateral surface of objects
Can grasp spherical or rounded items	Can grasp cylindrical/rectangular items
Highest load capacity: > 400 g	Highest load capacity: > 300 g
Cannot grasp cylindrical objects	Cannot grasp spherical objects

Chapter 4

Soft Aerial Vehicle Design and Control

This chapter focuses on the whole SAV system design and control. Since the two types of soft grippers (with or without the inextensible layers) have similar control strategies, this thesis would like to concentrate on the SAV with a soft gripper with the inextensible layers [38] as an example (excepted in Section 4.6 and 4.8).

4.1 Overall System Design

To simplify the grasping motion and overcome the complexity of controlling the countless degrees of freedom in soft robotics, a pneumatic soft gripper is equipped with four soft fingers that can be inflated or deflated simultaneously [32] by low-level feed-forward proportional control of pressure regulation (see Chapter 3). Hence, this proposed soft gripper is placed under the centre of gravity of a quadrotor and can grasp various target objects by controlling the inflation and deflation of its fingers.

All major components of the suggested SAV are depicted in Fig. 4.1 [38]. The flight controller, Holybro Kakute H7 v1.3, is capable of interacting with the onboard computer, Khadas VIM4, via the Robot operating system (ROS), thereby enhancing the real-time control efficiency of the SAV. Moreover, the durability of the SAV is enhanced by its air-

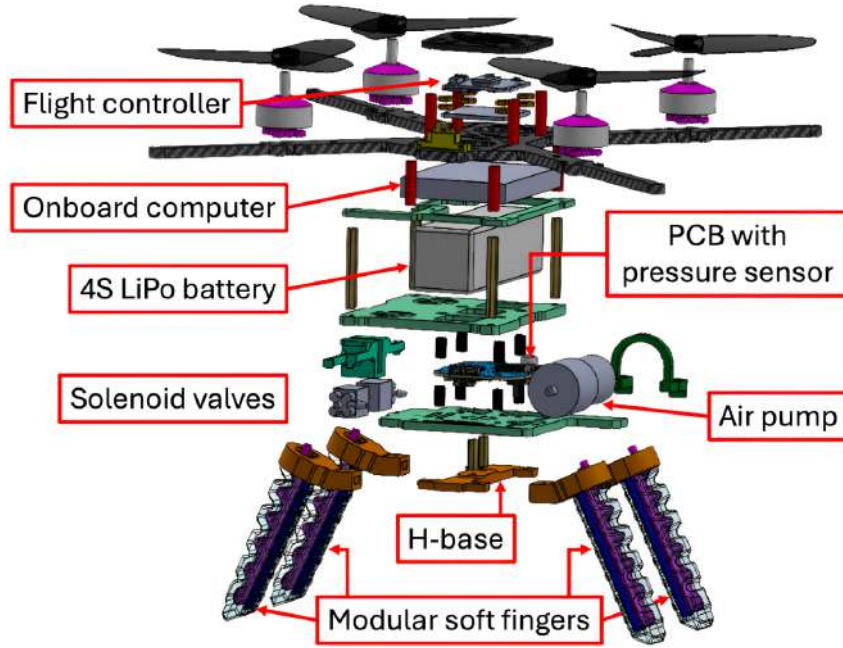


Figure 4.1: 3D CAD drawing of the exploded view of the proposed Soft aerial vehicle (SAV).

frame with a high strength-to-weight ratio of carbon fibre composites. This is a customized quadrotor base fabricated by CNC milling. Polylactic acid (PLA) is used in 3D printing to manufacture the remaining customised connecting boards due to the lightweight properties of the PLA. The SAV has a diagonal length of 385 mm and a height of 245 mm. The net weight of the quadrotor base of the SAV is 732 g, and the weight of the soft gripper remains the same in both configurations, 270 g.

4.2 System Dynamics

To simplify the dynamics of the SAV, the motion of the soft gripper during inflation and deflation are neglected [38]. Based on the characteristics of a conventional drone, we assume that the SAV can be treated as a rigid body with six degrees of freedom.

Fig. 4.2 illustrates the North-East-Down inertial frame, Γ_I and the body frame, Γ_B of the SAV.

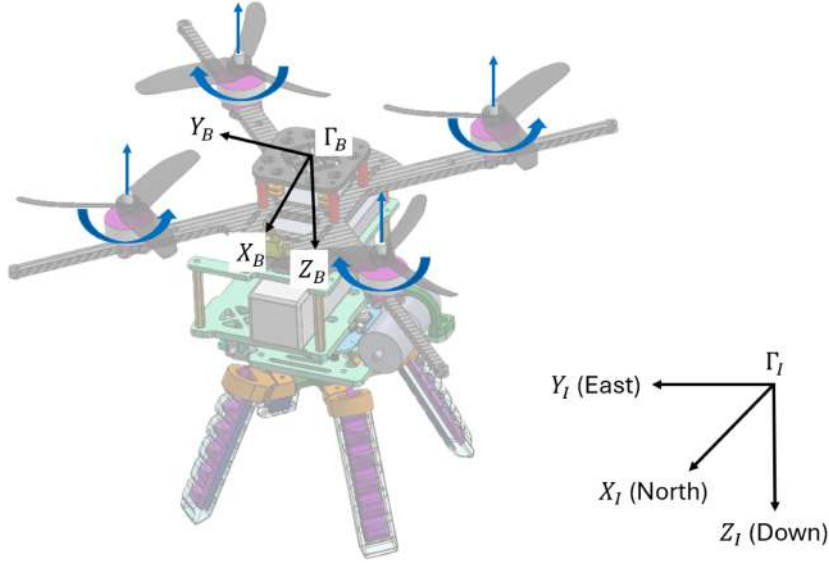


Figure 4.2: Soft aerial vehicle (SAV) sketch with its inertial frame Γ_I and body frame Γ_B .

As a result of the increased overall mass following grasping, the mass of the target objects will cause mass changes of the SAV. Also, several foreseeable external disturbances, such as the ground effect and the thrust dearth due to battery consumption, cannot be estimated precisely. The equivalent external disturbances δ that consists of the mass of the soft grasper, the mass change after grasping, the ground effect and the thrust dearth due to battery consumption is added in the mathematical model of the proposed SAV below. A disturbance observer is introduced in Section 4.3 to accurately estimate δ .

The mathematical model of the proposed SAV can be given by

$$\begin{aligned}
 \dot{\mathbf{P}} &= \mathbf{V}, \\
 \dot{\mathbf{V}} &= R(\Theta)(\mathbf{T} - \mathbf{g}) + \delta, \\
 \dot{\Theta} &= R(\Theta)\boldsymbol{\omega}, \\
 \dot{\boldsymbol{\omega}} &= \mathbf{I}^{-1}(\boldsymbol{\tau} - \boldsymbol{\omega} \times (\mathbf{I}\boldsymbol{\omega})),
 \end{aligned} \tag{4.1}$$

where $\mathbf{P} = [x, y, z]^\top$ and $\mathbf{V} = [u, v, w]^\top$ respectively represent the position and velocity of the UAV in Γ_I . $R(\Theta) \in \mathbb{R}^{3 \times 3}$ is the rotation matrix that can be found in [add a citation], $\Theta = [\phi, \theta, \psi]^\top$ is the attitude angle of the UAV, and $\boldsymbol{\omega} = [p, q, r]^\top$ is the angular rate

of the UAV defined in Γ_B . m is the mass, \mathbf{g} is the gravity force vector, $\mathbf{T} = [0, 0, T]^\top$, $\boldsymbol{\tau} = [\tau_x, \tau_y, \tau_z]^\top$, $I = \text{diag}(I_x, I_y, I_z)$ is the moment of inertia, and $\boldsymbol{\delta} = [\delta_x, \delta_y, \delta_z]^\top$ is the equivalent external disturbances defined in Γ_I .

4.3 Disturbance Observer Design

After the Soft aerial vehicle (SAV) grasps its target object, the total mass of the SAV will obviously increase due to the addition of the mass of the target object. Since the soft gripper is located beneath the centre of gravity of the SAV, the magnitude of δ_z is rapidly increased by the mass of the target item during aerial grasping, and the magnitudes of δ_x and δ_y are also affected when the SAV brings the target item to different setpoints. As a result, the dynamic model of the SAV will be changed after grasping, potentially leading to an unacceptable performance of the Nonlinear model predictive control (NMPC). However, this degradation can be mitigated by incorporating a disturbance observer in NMPC. The proposed disturbance observer aims to handle changes in dynamics arising from varying operational circumstances effectively. To ensure the comprehensiveness of the disturbance observer, the observer is designed to mitigate both expected and unexpected disturbances. This includes accounting for factors such as the mass of the target object while holding it in mid-air, environmental disturbances, and measurement noises. Therefore, linear acceleration disturbance, $\boldsymbol{\delta}$, is added to the original linear acceleration equations of the SAV's dynamic model (see Equation 4.1). By incorporating the disturbance observer, the NMPC system can accurately estimate and compensate for these disturbances, thereby enhancing the overall control performance of the SAV.

Recently, several research studies have focused on Model predictive control (MPC) with disturbance rejection [65] and disturbance observer [66–68] for UAVs or unmanned underwater vehicles. [69] mentioned the importance of adaptive MPC to compensate for model mismatch and prevent degraded performance.

Thereby, this thesis proposes and tests two disturbance observers in aerial grasping. One utilises an Extended Kalman filter (EKF) while another one uses a Three-order robust differentiator (RD3) [70]. The objective of both observers is to estimate and compensate for disturbances that may impact the dynamics of the aerial grasping system. The estimated disturbances obtained from these observers can be effectively incorporated into the prediction horizon of the NMPC algorithm and updated at each time step. By considering the estimated disturbances during the control optimisation process, the NMPC can generate optimal control inputs that effectively reject disturbances and enhance the overall performance of the aerial grasping system. Through testing and evaluation, the performance and effectiveness of both disturbance observers can be assessed in the specific context of aerial grasping applications, verifying their capabilities to estimate and compensate for disturbances and their impact on the NMPC control strategy.

4.3.1 Disturbance Observer Using an Extended Kalman Filter

EKF is a widely used estimation algorithm that combines a linearised dynamic model with measurement data to estimate system states [71,72]. By incorporating the EKF into the disturbance observer, it becomes possible to effectively estimate disturbances on sensor measurements, including position coordinates of the SAV \mathbf{P} obtained from a motion capture system, linear velocity \mathbf{V} of the SAV from sensors in the flight controller, and linear acceleration of the SAV, $\tilde{\mathbf{a}}_{\mathbf{B}} = [\tilde{u}_B, \tilde{v}_B, \tilde{w}_B] \in \mathbb{R}^3$, from the Initial measurement unit (IMU) in the flight controller. The effects of the prediction states and the measurement states of the SAV can be tuned by changing covariances. The system states χ and measurement states ζ of the SAV can be presented as:

$$\chi = [\mathbf{P}, \mathbf{V}, \hat{\delta}_{\mathbf{B}}]^T \quad (4.2)$$

$$\zeta = [\mathbf{P}, \mathbf{V}, \tilde{\mathbf{a}}_{\mathbf{B}}]^T \quad (4.3)$$

where $\hat{\delta}_{\mathbf{B}} = [\hat{\delta}_{B_x}, \hat{\delta}_{B_y}, \hat{\delta}_{B_z}] \in \mathbb{R}^3$ denotes the predicted linear acceleration disturbance in the body frame of the SAV.

Therefore, the system dynamics function is defined as follows:

$$f(\chi, u) = [\mathbf{V}, \tilde{\mathbf{a}}_{\mathbf{B}}, \hat{\delta}_{\mathbf{B}}]^T \quad (4.4)$$

It is worth noting that the accuracy estimation of the linear acceleration disturbance mainly varies inversely with the amount of noise present in the IMU. In other words, if the noise in the IMU decreases, the accuracy of the estimated linear acceleration disturbance improves. This highlights the importance of having a reliable and accurate IMU to enhance the disturbance estimation process and subsequently improve the overall performance of the aerial grasping system. Thus, the process noise covariance matrix \mathbf{Q} and the measurement noise covariance matrix \mathbf{R} are tuned to get a satisfied disturbance estimation. The two covariances are computed as follows:

$$\mathbf{Q} = \text{diag} \left[\frac{(\Delta t)^{q_p}}{q_p} \quad \frac{(\Delta t)^{q_v}}{q_v} \quad (\Delta t)^{q_\delta} \right] \quad (4.5)$$

$$\mathbf{R} = \text{diag} \left[(\Delta t)^{r_p} \quad (\Delta t)^{r_v} \quad \frac{(\Delta t)^{r_{\tilde{\mathbf{a}}}}}{r_{\tilde{\mathbf{a}}}} \right] \quad (4.6)$$

where \mathbf{Q}, \mathbf{R} are 9×9 matrices, $\text{diag} \frac{(\Delta t)^{q_p}}{q_p}$, $\text{diag} \frac{(\Delta t)^{q_v}}{q_v}$, $\text{diag}(\Delta t)^{q_\delta}$, $\text{diag}(\Delta t)^{r_p}$, $\text{diag}(\Delta t)^{r_v}$, $\text{diag} \frac{(\Delta t)^{r_{\tilde{\mathbf{a}}}}}{r_{\tilde{\mathbf{a}}}}$ are 3×3 matrices, Δt is the sample time step, which is 0.01 second.

By our observation, the position and velocity measurements of the SAV from the indoor motion capture system and the Flight control unit (FCU) are reliable and not noisy. In contrast, the linear acceleration data from IMU is quite noisy. As a result, the predicted linear acceleration results should be more reliable than those from the

measurement model, while the measured position and velocity results are more reliable than those from the prediction model. The values of the two covariance matrices are tuned according to the experimental results for getting the fastest and stable response of the SAV's motion tracking during the integration of the observer with the NMPC. Thus, the parameters of the two covariance matrices are determined below:

$$\begin{aligned}
 q_p &= q_v & &= r_{\tilde{a}} = 2 \\
 r_p &= r_v & &= 4 \\
 q_\delta &= [4.2, 4.2, 3.5]
 \end{aligned} \tag{4.7}$$

In the prediction step, we compute the Jacobian of the system dynamics and predict the next state using a 4th-order Runge-Kutta (RK4) method as:

$$\begin{aligned}
 \chi_{k+1} &= f(\chi, \hat{\mathbf{d}}_{\mathbf{B}}, k) = \chi_k + \frac{1}{6}(K_1 + 2K_2 + 2K_3 + K_4) \\
 K_1 &= \Delta k \cdot f(\chi_k, \hat{\mathbf{d}}_{\mathbf{B}}) \\
 K_2 &= \Delta k \cdot f\left(\chi_k + \frac{K_1}{2}, \hat{\mathbf{d}}_{\mathbf{B}}\right) \\
 K_3 &= \Delta k \cdot f\left(\chi_k + \frac{K_2}{2}, \hat{\mathbf{d}}_{\mathbf{B}}\right) \\
 K_4 &= \Delta k \cdot f\left(\chi_k + K_3, \hat{\mathbf{d}}_{\mathbf{B}}\right)
 \end{aligned} \tag{4.8}$$

The Jacobian of the system dynamics \mathbb{F} and covariance prediction $\mathbb{P}_{k-1|k}$ are computed in Equations 4.9 and 4.10.

$$\mathbb{F}_k = \left. \frac{\partial f}{\partial \chi} \right|_{\chi_k, u_k} \tag{4.9}$$

$$\mathbb{P}_{k|k-1} = \mathbb{F}\mathbb{P}_k\mathbb{F}^T + Q \tag{4.10}$$

The Jacobian of measurement model \mathbb{H} , and measurement residual $\hat{y}_{k|k}$ are formulated as the Equations 4.11 and 4.12, where z_k is the actual measurement.

$$\mathbb{H}_k = \left. \frac{\partial h}{\partial \chi} \right|_{\chi_{k|k-1}} \quad (4.11)$$

$$\hat{y}_{k|k} = z_k - h(\hat{\chi}_{k|k-1}) \quad (4.12)$$

Then the Kalman Gain \mathbb{K} at time k can be computed according to $\mathbb{P}_{k|k-1}$ and \mathbb{H}_k . Eventually, the state estimate $\hat{\chi}_{k|k}$ can be updated by the predicted state estimate $\hat{\chi}_{k|k-1}$ and \mathbb{K} , and then recalculate $\mathbb{P}_{k|k}$ by K_k and \mathbb{H}_k .

$$\begin{aligned} K_k &= \mathbb{P}_{k|k-1} \mathbb{H}_k^T (\mathbb{H}_k \mathbb{P}_{k|k-1} \mathbb{H}_k^T + R_k)^{-1} \\ \hat{\chi}_{k|k} &= \hat{\chi}_{k|k-1} + K_k \hat{y}_{k|k} \\ \mathbb{P}_{k|k} &= (I - K_k \mathbb{H}_k) \mathbb{P}_{k|k-1} \end{aligned} \quad (4.13)$$

4.3.2 Disturbance Observer Using a Three-order Robust Differentiator

RD3 [70,73,74] is a fixed time fractional-order differentiator that is robust to measurement noise and capable of accurately estimating disturbances in dynamic systems. By utilizing RD3 as the disturbance observer, the goal is to provide reliable disturbance estimation and compensation for the aerial grasping system. Unlike the EKF, RD3 relies only on position information from the motion capture system and linear acceleration from the thrust model to predict linear acceleration disturbances. Thus, it can avoid the effects caused by the noise of the IMU. The adjustment of the gain values of RD3 can be simply done by tuning some parameter, which is intuitive and effective. Moreover, RD3 is an observer with fixed-time convergence, meaning that theoretically, when the time exceeds a certain threshold, RD3 can track any form of a complex signal.

The RD3-based observer can be given by

$$\begin{aligned}
 \dot{\mu}_1 &= \mu_2 + m_1[\tilde{e}_\eta/k_0]^{3/4} + n_1[\tilde{e}_\eta/k_0]^{5/4}, \\
 \dot{\mu}_2 &= \mu_3 - \frac{k_t}{m}\dot{\eta} + u_\eta - \ddot{\eta}_d + m_2[\tilde{e}_\eta/k_0]^{2/4} + n_2[\tilde{e}_\eta/k_0]^{6/4}, \\
 \dot{\mu}_3 &= m_3[\tilde{e}_\eta/k_0]^{1/4} + n_3[\tilde{e}_\eta/k_0]^{7/4}
 \end{aligned} \tag{4.14}$$

where μ_1 , μ_2 , and μ_3 are the estimation of the position, velocity, and equivalent external disturbance of the quadrotor, respectively. k_0 is a scalar factor to adjust the accuracy of the observer, k_t is the linear damping coefficient, m is the mass, η is the position of the quadrotor, e_η is the tracking error of η , and \tilde{e}_η is the estimation of η .

Additionally, to guarantee the fixed-time convergence, hyper-parameters $m_1, m_2, m_3, n_1, n_2, n_3$ should be selected such that matrices A_m and A_n are Hurwitz.

$$A_m = \begin{bmatrix} -m_1 & 1 & 0 \\ -m_2 & 0 & 1 \\ -m_3 & 0 & 0 \end{bmatrix} \quad A_n = \begin{bmatrix} -n_1 & 1 & 0 \\ -n_2 & 0 & 1 \\ -n_3 & 0 & 0 \end{bmatrix} \tag{4.15}$$

For ease of the determination of those hyper-parameters, we use the characteristic of the solution of a third-order polynomial, which can be yielded as

$$\begin{aligned}
 &(s + \omega_1)(s + \omega_2)(s + \omega_3) \\
 &= s^3 + (\omega_1 + \omega_2 + \omega_3)s^2 + (\omega_1\omega_2 + \omega_1\omega_3 + \omega_2\omega_3)s + \omega_1\omega_2\omega_3 = 0
 \end{aligned} \tag{4.16}$$

where ω_1, ω_2 , and ω_3 are the three roots of the Equation 4.16.

Note the fact that the characteristic polynomials of matrices A_m and A_n can be respectively given by solving equation $\det A_\kappa - sI_3 = 0, \kappa = m, n$, which yields

$$\begin{aligned}
 s^3 + m_1s^2 + m_2s + m_3 &= 0, \\
 s^3 + n_1s^2 + n_2s + n_3 &= 0
 \end{aligned} \tag{4.17}$$

Evidently, it indicates that

$$\begin{aligned}
 m_1 &= \omega_1 + \omega_2 + \omega_3, \\
 m_2 &= \omega_1\omega_2 + \omega_1\omega_3 + \omega_2\omega_3, \\
 m_3 &= \omega_1\omega_2\omega_3
 \end{aligned}
 \tag{4.18}$$

4.3.3 Observers Performance Test

To evaluate the performance of the Disturbance observer-based nonlinear model predictive control (DOMPC), the SAV carried an additional 257 g payload (a 4S LiPo battery) and followed a lemniscate trajectory with an amplitude of 2 m, frequency of 1 Hz and an altitude of 1.0 m by NMPC with the above disturbance observers using EKF and RD3, respectively. Fig. 4.3 illustrates the trajectories of the SAV when the two proposed disturbance observers were applied to it, respectively (NMPC-EKF and NMPC-RD3). The flight tests were conducted under a VICON motion capture system, which provided real-time ground truth data to assist the flight controller in tracking the designated setpoints. In Fig. 4.5, the load was positioned off-centre from the SAV's centre of gravity, next to the original SAV's battery, to add additional unpredictable variables to the system.

The resulting statistics for the position tracking performance in this observer comparison are given in Fig. 4.4. The NMPC-EKF and NMPC-RD3 got similar tracking performance, especially in the x and y directions. However, for the z-direction tracking, although the tracking position of NMPC-RD3 was close to the reference, 1 m, it could not reach 1 m again after getting a slightly higher altitude. In contrast, the NMPC-EKF could reach the reference altitude repeatably during the test. Consequently, the proposed disturbance observer utilises EKF should be chosen to integrate the NMPC in the next section.

Referring to Fig. 4.4, the disturbance observer that using RD3 cannot perform as

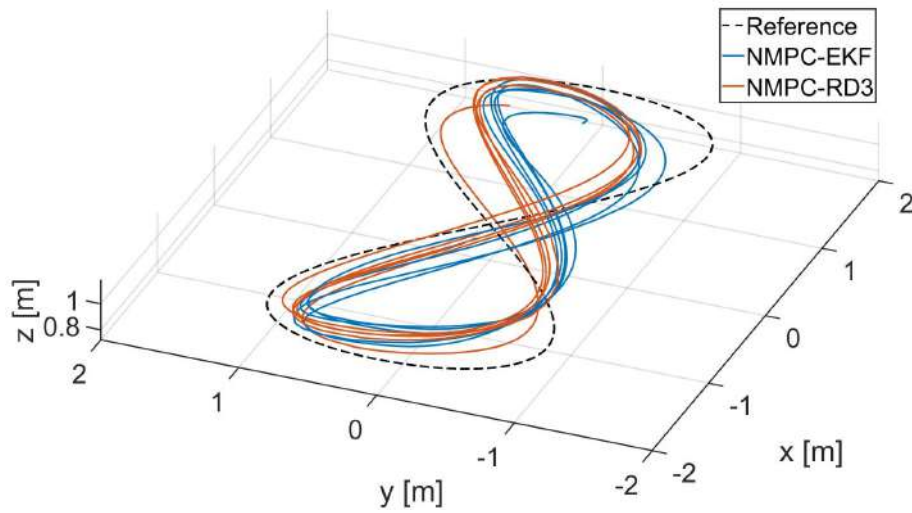


Figure 4.3: Trajectories results of the SAV lemniscate flights under the application of NMPC-EKF and NMPC-RD3.

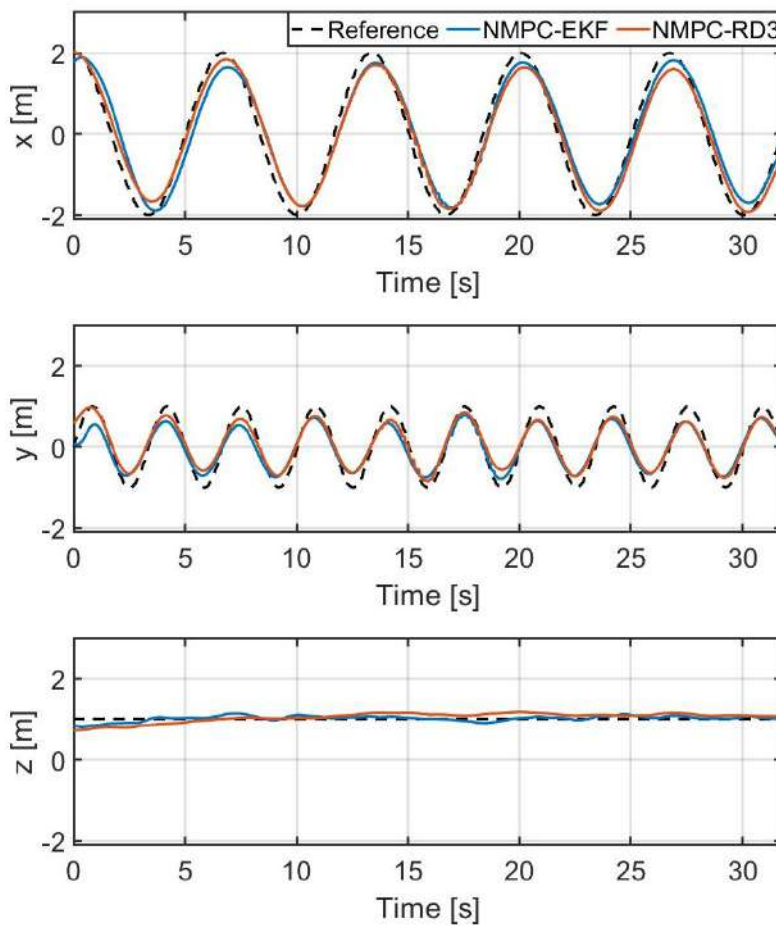


Figure 4.4: Position tracking performance of the SAV Lemniscate flights with an additional 257g load using NMPC-EKF and NMPC-RD3 along the x , y , and z axes.

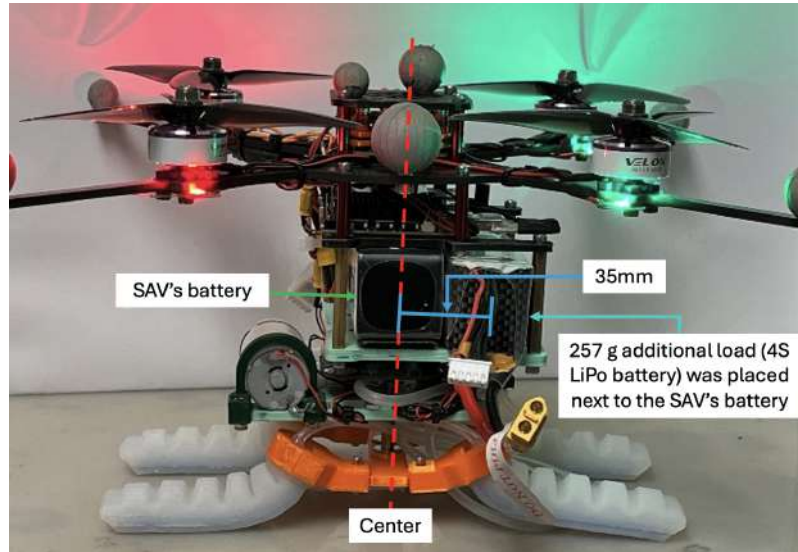


Figure 4.5: A 257 g off-centered load is placed next to the battery of the SAV. The distance between the center of the SAV and the center of the load is 35 mm.

precisely as the existing research [70, 73]. This may be because the sliding mode controller in [70, 73] also compensates for the dynamics change of the Unmanned aerial vehicle (UAV). Thus, this observer can function better with a sliding mode controller instead of NMPC.

4.4 Disturbance Observer-Based Nonlinear Model Predictive Control

After the Soft aerial vehicle (SAV) grasps its target object, the total mass of the SAV increases due to the addition of the mass of the target object [38]. Consequently, the dynamic model of the SAV changes, potentially resulting in degraded performance of the Nonlinear model predictive control (NMPC). However, this degradation can be mitigated by incorporating a disturbance observer in the NMPC. The proposed disturbance observer, described in Section 4.3.1, effectively handles changes in dynamics that arise from varying operational circumstances. To account for these changes, linear acceleration dis-

turbances are added to the linear acceleration equations of the SAV's dynamic model in Equation (4.1) and the nonlinear prediction model in its NMPC controller in Equation (4.19). These disturbances are transformed from Γ_B to Γ_I by multiplying the rotation matrix. By incorporating the disturbance observer, the NMPC system can accurately estimate and compensate for these disturbances, thereby enhancing the overall control performance of the SAV. The cascaded control structure of the Disturbance observer-based nonlinear model predictive control (DOMPC) is described in Fig. 4.6, while the finite state machine diagram is illustrated in Fig. 4.9.

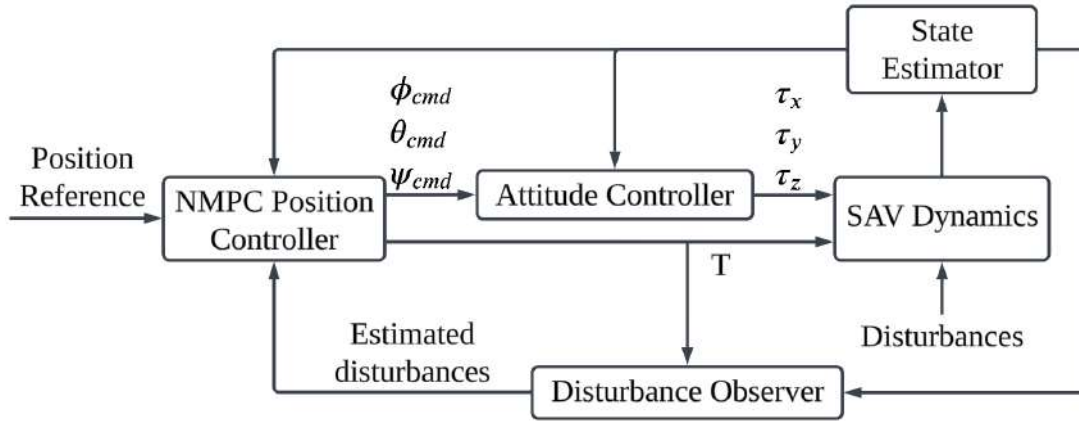


Figure 4.6: Cascaded loop control structure of disturbance observer-based NMPC (DOMPC).

Referring to [39], after adding the estimated disturbance from the proposed disturbance observer (using Extended Kalman filter (EKF)) in Section 4.3.1, the nonlinear prediction model in the NMPC controller is formulated as follows:

$$\begin{cases} \dot{\mathbf{P}} = \mathbf{V} \\ \dot{\mathbf{V}} = R(\Theta) * (\mathbf{T} - g) + \delta \\ \dot{\phi} = \frac{\phi_{cmd} - \phi}{\tau_{\phi}} \\ \dot{\theta} = \frac{\theta_{cmd} - \theta}{\tau_{\theta}} \end{cases} \quad (4.19)$$

where τ_{ϕ} and τ_{θ} are time constants of roll and pitch control, ϕ_{cmd} and θ_{cmd} are roll and

pitch commands sent to inner loop attitude control. The yaw angle is not included in the above NMPC states as the inner loop controller controls the yaw angle. The system identification technique can be used with flight data to derive the values of τ_ϕ and τ_θ .

The estimated disturbances obtained from the disturbance observer can be effectively incorporated into the prediction horizon N of the NMPC algorithm and updated at each time step. By considering the estimated disturbances during the control optimization process, the NMPC can generate optimal control inputs that effectively reject disturbances and enhance the overall performance of the aerial grasping system.

The optimizer solves the Quadratic programming (QP) problem formulated as [39]:

$$\begin{aligned}
 \min \quad & \int_{t=0}^N \|h(x(t), u(t)) - y_{ref}\|_Q^2 dt \\
 & + \|h(x(T)) - y_{N,ref}\|_{Q_N}^2 dt \\
 \text{s.t.} \quad & \dot{x} = f(x(t), u(t)) \\
 & u(t) \in \mathbb{U} \\
 & x(t) \in \mathbb{X} \\
 & x(0) = x(t_0),
 \end{aligned} \tag{4.20}$$

where $u(t)$ and $x(t)$ represent the control input and state at timestep t , respectively. y_{ref} and $y_{N,ref}$ denote the reference state for the prediction horizon and terminal timestep, respectively. Q and Q_N represent the weighting matrices for states and terminal states, while $f(\cdot)$ and $h(\cdot)$ indicate the prediction function and system output function, respectively. \mathbb{U} and \mathbb{X} are the input constraint and state constraint.

The Optimal control problem (OCP) in Eq. (4.20) is solved using the Multiple Shooting Method with the Active Set Method and qpOASES solver, employing the Sequential Quadratic Programming (SQP) technique [37]. Real-time computation is achieved through the implementation of NMPC with the Automatic control and dynamic optimization (ACADO)" solver, which offers efficient solutions for estimation and optimal

control problems [75].

4.4.1 Controller adaptability Test

To evaluate the performance of the DOMPC, the SAV carried a 257 g payload (a 4S LiPo battery) and followed a circular trajectory with a radius of 1.8 m at a speed of 2 m/s and an altitude of 1.0 m by DOMPC, NMPC, and Proportion-Integration-Differentiation (PID) respectively. The flight tests were conducted under a VICON motion capture system, which provided real-time ground truth data to assist the flight controller in tracking the target setpoints. The load was positioned off-centre from the SAV's centre of gravity next to the SAV's battery.

The resulting statistics for the position tracking performance are given in Fig. 4.7. The DOMPC has better tracking performance in the x and y directions and has similar tracking performance with the PID controller in the z-direction. However, due to the latency of the PID controller in the x and y directions, it could not perform as well as the DOMPC controller. In contrast, the NMPC controller showed significant tracking errors, particularly in the z-direction, as it could only maintain its altitude at around 0.5 meters. In Fig. 4.8, the tracking performance of NMPC controller in the z-direction was the worst as the SAV flew much lower than the desired altitude. On the other hand, SAV with DOMPC and PID controllers could reach the desired altitude of this circular trajectory successfully. Hence, adding the proposed disturbance observer to NMPC is the most effective method for compensating the dynamic changes of the SAV and ensuring accurate path tracking while only using the NMPC and PID controllers is less robust for handling dynamic changes due to unknown payloads.

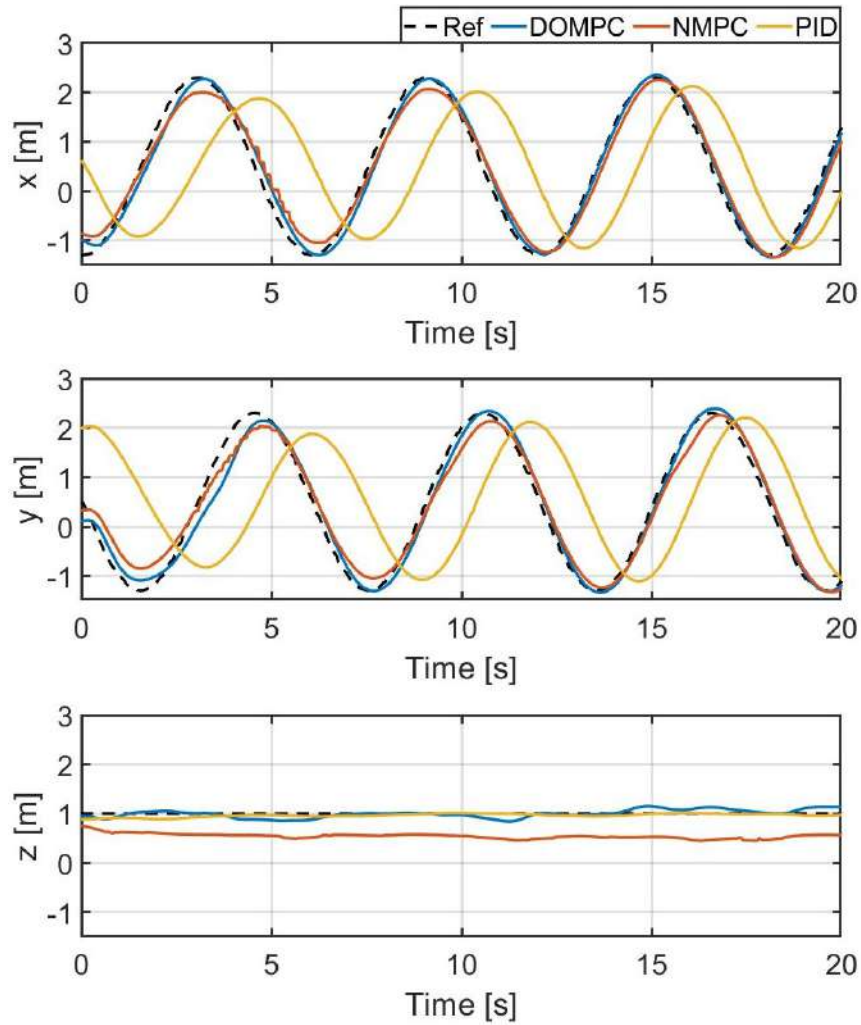


Figure 4.7: Position tracking performance of the SAV circular flights with an additional 257g load using DOMPC, NMPC, and PID along the x, y, and z axes.

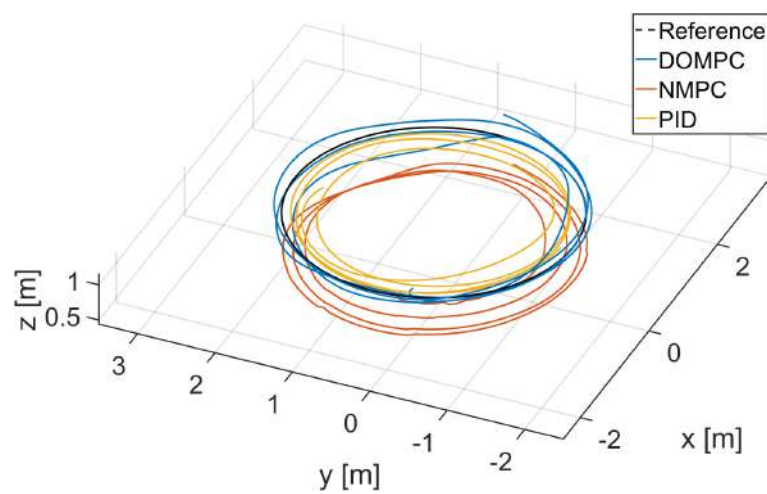


Figure 4.8: Trajectories results of the SAV circular flights.

4.5 Finite State Machine for Aerial Grasping mission

A Finite state machine (FSM) module [76] aims to assist Soft aerial vehicle (SAV) in different stages to completing the aerial grasping. There are six stages in total, including not only the grasping of the target item, but also the releasing of the item before landing. Here is the list of the six stages:

1. Takeoff and waiting for position data of target object.
2. Approaching the target object.
3. Grasping the target object at the desired grasp point.
4. Lifting the target object object to the desired hovering point.
5. Releasing the target object at the releasing destination.
6. Landing.

Fig. 4.9 describes the FSM diagram and indicates that the application of the proposed disturbance observer is excluded during takeoff (first stage) and landing (Sixth stage). The estimated disturbance would not be utilized during these two stages for mitigating the ground effect, friction, and contact force experienced by the SAV [38]. The trajectory of the aerial grasping mission with the six stages is presented in Fig. 4.10.

4.5.1 First stage: Takeoff and waiting for position data of target object

In the first stage, the onboard computer on the SAV initially sends the deflation command to the microcontroller of the soft gripper so that the soft gripper acts as the soft

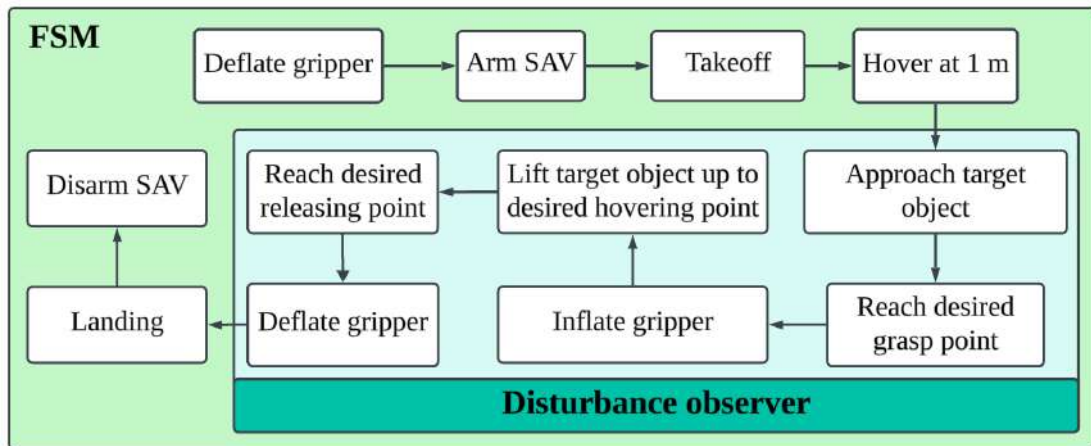


Figure 4.9: Finite state machine diagram for the SAV aerial grasping task.

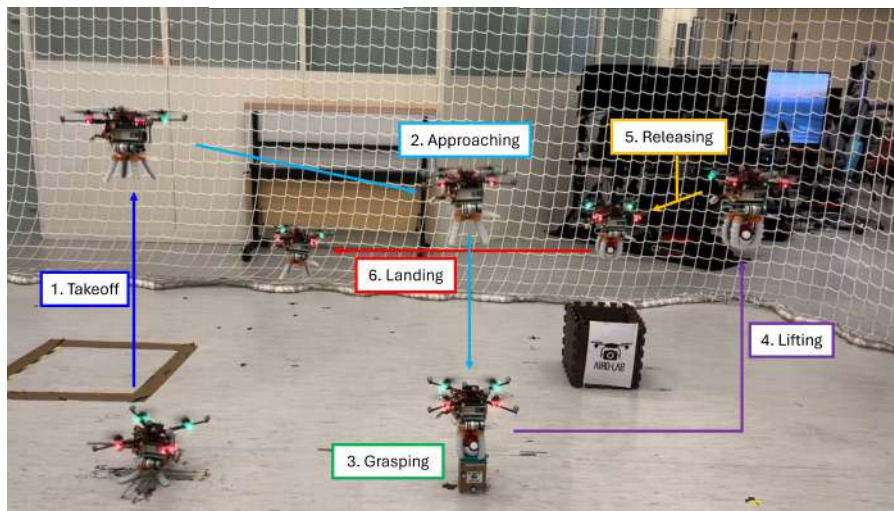


Figure 4.10: Trajectory of the aerial grasping mission.

landing gear before taking off. The desired takeoff altitude is at 1 m. After it reaches the desired altitude, it hovers and waits for the position data of the target object. The static translational offset of an object between its body frame (estimated by VICON) and its centre of mass requires manual calibration. This is necessary because the body frame of the object depends on the locations of the reflective markers, which are attached to the stands of the objects, for the ease of repeating the grasping task with various target items.

4.5.2 Second stage: Approaching the target object

When SAV receives the target object's location, it starts approaching the target object by hovering over the object. Sustaining the x and y directions based on the target object's location, it gradually decreases its altitude to be close to the object. The soft gripper keeps receiving the deflation command to provide the maximum grasping tolerance.

4.5.3 Third stage: Grasping the target object at the desired grasp point

The soft gripper inflates to grasp the target object after the SAV reaches the desired grasp point. The SAV preserves hovering at the desired grasp point to secure the grasp. The estimated linear acceleration disturbance along the z direction starts to increase due to the weight of the target object.

4.5.4 Forth stage: Lifting the target object object to a desired hovering point

The SAV lifts the target object to a desired hovering point for analysing the performance of the proposed disturbance observer. Since the net weight of the SAV rapidly increase due to the extra weight of the payload, the SAV requires more time to compensate for the linear acceleration disturbances by its DOMPC.

4.5.5 Fifth stage: Releasing the target object at the releasing destination

A basket built with five puzzle foam mats is placed on the releasing destination. After switching to this stage, the SAV holds the object to the top of this basket. When it reaches the desired setpoint, the soft gripper deflates again to release the object.

4.5.6 Sixth stage: Landing

After the object is released by the deflation of the soft gripper, the SAV goes to the last setpoint to prepare for landing. The soft gripper's deflation remains so that the soft gripper can act as the soft landing gear again. The SAV gradually decreases its altitude at the landing setpoint and disarms its four brushless motors when it lands on the ground solidly.

4.6 Payload Test

The primary objective of this test was to evaluate the payload capacity of the Soft aerial vehicle (SAV), intentionally excluding the assessment of its aerial grasping capability. From [32], the SAV successfully grasped a 217 g double-sided tape using the X-base soft gripper and a 217 g plastic cylindrical container using the H-base soft gripper in Fig. 4.11. Referring to [38], to ascertain the maximum payload capacity of the SAV, it not only carried the same load utilized in the observer performance test during mid-air operation, but also grasped a container with varying weights while hovering.

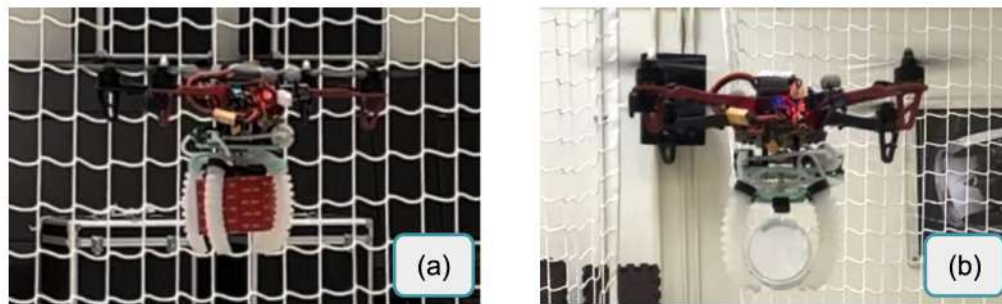


Figure 4.11: Payload test of the SAV with its soft gripper (without inextensible layers): hovering after holding a 217 g payload in total with its (a) X-base and (b) H-base soft gripper, respectively.

In Fig. 4.12(a), the SAV could carry a 337 plastic box and a 257 g extra payload simultaneously with its H-base soft gripper [38]. Similar payload capacity of the SAV is shown in Fig. 4.12(b) too. The SAV could carry a 224 g spherical container and the same 257 g extra payload simultaneously with its X-base soft gripper that contains inextensible layers. The payload tests in Fig. 4.11 and 4.12 were conducted for over 30 seconds. The highest resultant payload capacity (634 g) in Fig. 4.12(a) surpasses that of several existing research projects, such as a 100 g payload in [7], a 106 g foam target in [3], a 148 g med-kit in [59], and a 150 g packet in [8]. The accompanying video in Section 6.2 demonstrates these four payload tests.

The payload test results also indicate that the higher net weight of the SAV with the

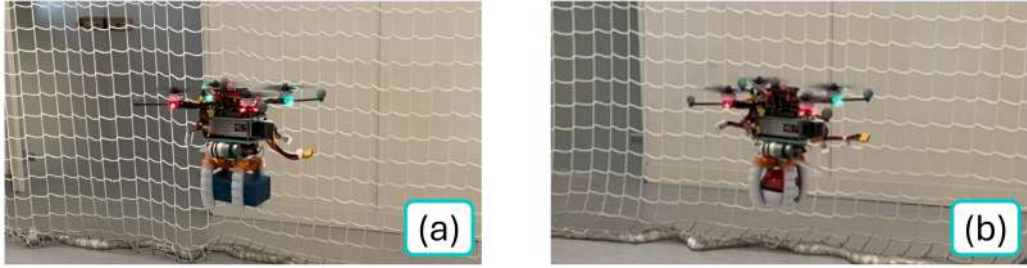


Figure 4.12: Payload test of the SAV with its soft gripper (with inextensible layers): (a) hovering after carrying a 634 g payload in total with its H-base soft gripper. (b) hovering after carrying a 481 g payload in total with its X-base soft gripper.

soft gripper that contains inextensible layers does not decline its payload capacity (1002 g SAV in [38] and 808 g SAV in [32]). In contrast, the payload capacity shown in Fig. 4.12 is more than double that in Fig. 4.11. The increase in the payload capacity is caused by the higher pinching force of the soft gripper with inextensible layers. Consequently, the soft gripper's gripping force is a critical factors in the payload test.

To further analyze the SAV position tracking performance with the proposed Disturbance observer-based nonlinear model predictive control (DOMPC) during the payload test, the position tracking records of the SAV [38] in Fig. 4.12 during adding and releasing payloads are described as follows.

4.6.1 Position Tracking Results of SAV with H-base Soft Gripper (With Inextensible Layer)

Following the SAV's hover, the plastic box was initially positioned beneath it for grasping. The maximum weight of the box was 337 g in Fig. 4.12. Subsequently, after the SAV grabbed the box and returned to the desired hovering point, the additional 257 g load was placed next to its battery. The box was released after the SAV reached the target hovering point with both the box and the load. Similarly, the load was removed after the SAV resumed hovering at the desired point.

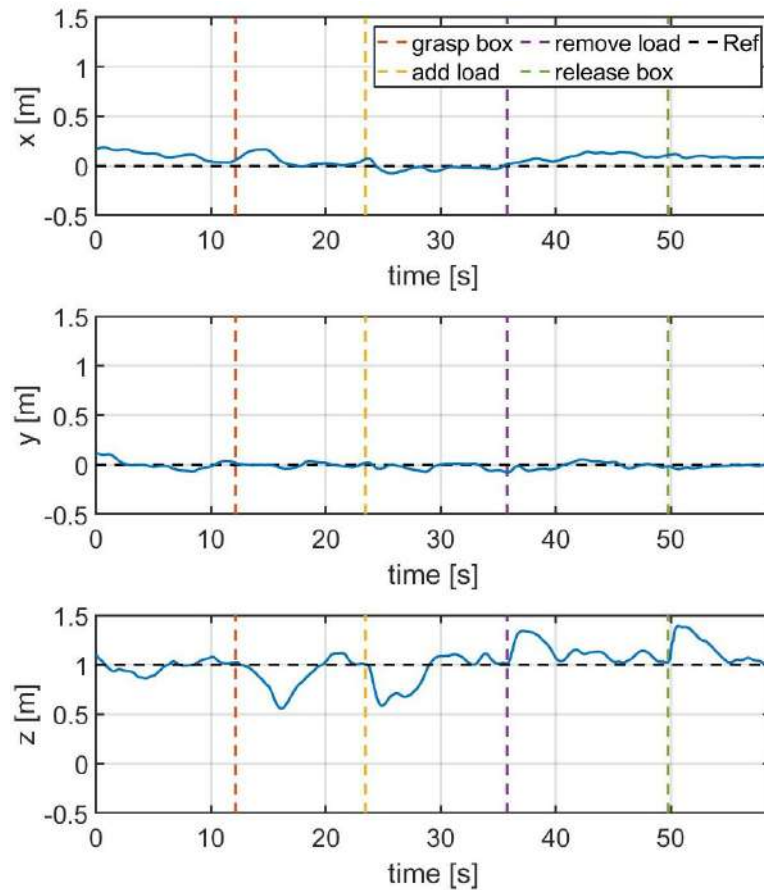


Figure 4.13: Position tracking performance along the x, y, and z axes in the payload test of the SAV with its H-base soft gripper.

Figure 4.13 illustrates the position tracking of the SAV. During this payload test, although the altitude of the SAV decreased when it began grasping the box and carrying the load, it ultimately maintained its hovering position with the proposed disturbance observer. Its hovering position was also sustained when its payload was released or removed.

4.6.2 Position Tracking Results of SAV with X-base Soft Gripper (With Inextensible Layer)

Using the same approach in Section 4.6.1, following the SAV's hover, the spherical container was initially positioned beneath it for grasping. The maximum weight of the container was 224 g in Fig. 4.12. Then, after the SAV grabbed the ball and returned to the desired hovering point, the additional 257 g load was placed next to its battery. The ball was released after the SAV reached the target hovering point with both the ball and the load. Likewise, the load was removed after the SAV resumed hovering at the desired point.

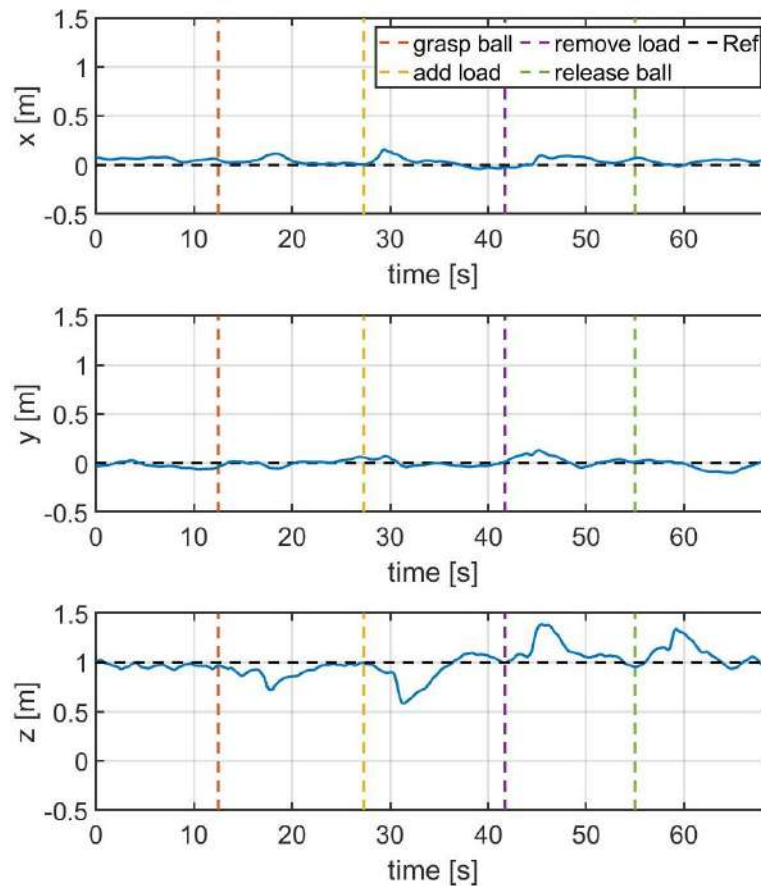


Figure 4.14: Position tracking performance along the x, y, and z axes in the payload test of the SAV with its X-base soft gripper.

Figure 4.14 illustrates the position tracking of the SAV. The results of this payload test are close to the previous payload test with an H-base soft gripper. While the SAV's altitude initially dropped upon grasping the ball and bearing the load, it successfully maintained its hovering position using the proposed disturbance observer. The hovering stability persisted even when the payload was released or removed.

4.7 Soft Aerial Grasping Test

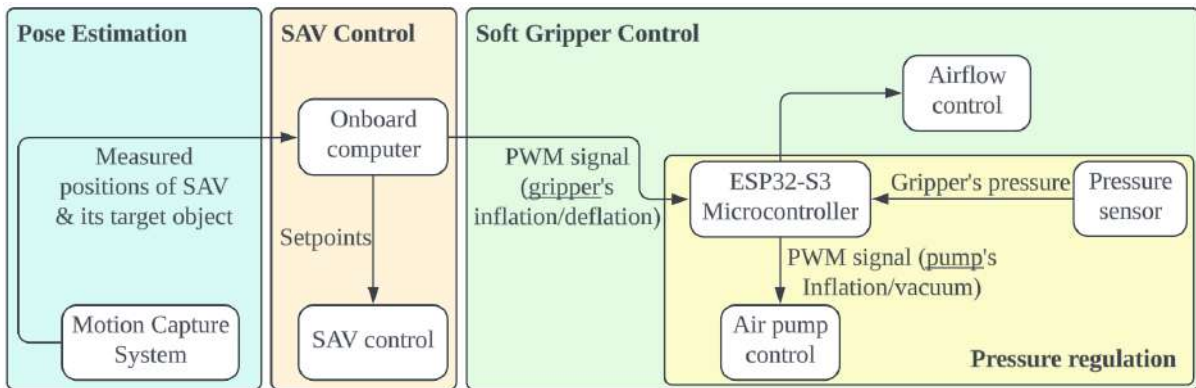


Figure 4.15: Grasping pipeline overview of the proposed soft aerial grasping.

In the aerial grasping task [38], we tested the aerial grasping ability of the Soft aerial vehicle (SAV) with both static and non-static payloads. For the target objects preparation, we placed extra loads into a spherical container, stuck additional loads on the side of the cylindrical shuttlecock tube, and poured dyed water into a rectangular plastic water bottle. The dimensions and weights of the three target objects can be found in Table 4.1, and the loads' positions of the objects are shown in Fig. 4.16. The X-base soft gripper handled the spherical container, while the H-base soft gripper handled the cylindrical shuttlecock tube and rectangular plastic bottle with dyed water. Despite experiencing slight tracking errors during the grasping process, the softness of the gripper compensated for these errors, providing sufficient grasping tolerance. As a result, the target objects were securely grasped without any damage [32].

Table 4.1: Dimensions and weights of target objects.

Target objects	Dimensions/Volumes	Weights (g)
Shuttlecock Tube with 46 g load	$238 \text{ mm} * (33 \text{ mm})^2 \pi$	113
Spherical container with 118 g load	$\frac{4}{3} \pi * (35 \text{ mm})^3$	161
Plastic bottle with 80 g dyed water	$210 \text{ mm} * 60 \text{ mm} * 60 \text{ mm}$	110



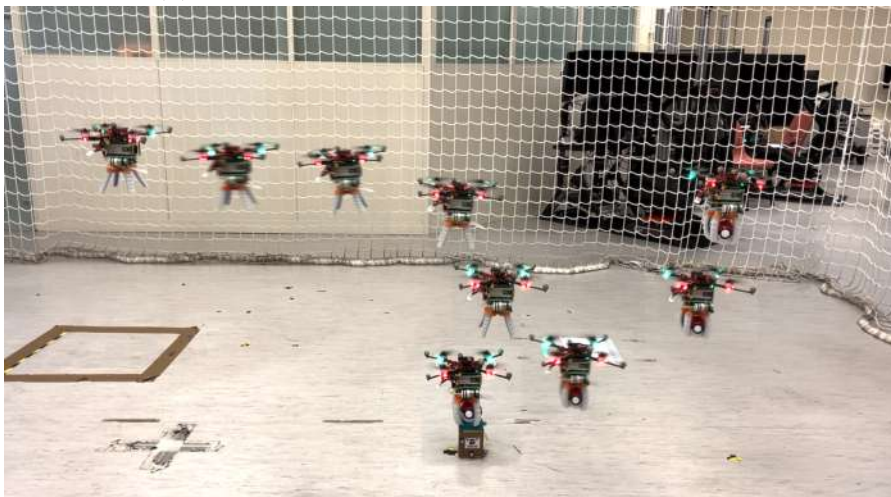
Figure 4.16: Three target objects: (a) Spherical container with loads. (b) Shuttlecock tube with its slide loads. (c) Plastic bottle with dyed water

Since this work focuses on the disturbance observer’s ability to estimate unknown payload and other uncertainties that can affect the dynamics of the SAV, we did not provide a predefined trajectory for the SAV during the aerial grasping task. Instead, we instructed the SAV to fly point-to-point, evaluating its ability to reach the desired points with low tracking errors. Before takeoff, the soft gripper received a deflation command from the flight controller via Robot operating system (ROS). After successfully reaching the desired grasping point, the flight controller sent a Pulse-width modulation (PWM) command for inflation to the soft gripper’s controller. The SAV remained in position for at least 5 seconds to ensure the soft gripper was fully inflated, thereby testing its ability to overcome the ground effect.

With the proposed disturbance observer [38], Fig. 4.17 illustrates the successful aerial grasping demonstrations performed by the SAV. Equipped with Disturbance observer-based nonlinear model predictive control (DOMPC), the SAV demonstrates precise hovering capabilities over target objects and effectively grasps them at the desired location. Referring to Fig. 4.10 and Section 4.5, after takeoff, the SAV approached its target object



(a) grasping a shuttlecock tube with 46 g load.



(b) grasping a spherical container with 118 g load.



(c) grasping a plastic bottle with 80 g.

Figure 4.17: Trajectories of grasping the three targets.

by decreasing its altitude accordingly. Fig. 4.18 shows that as the SAV was instructed to transport the target object along the x-axis at a height of 1 m following grasping, the magnitude of tracking errors along the z-axis and x-axis rapidly increased after grasping the three target objects, respectively. The tracking errors for the three aerial grasping tasks were much smaller because the SAV was required to fly along the x-axis only to grasp and lift the corresponding target objects. However, due to the disturbance detection capability of DOMPC, these errors quickly converged toward zero. The soft gripper finished inflation for grasping at 13.1 s.

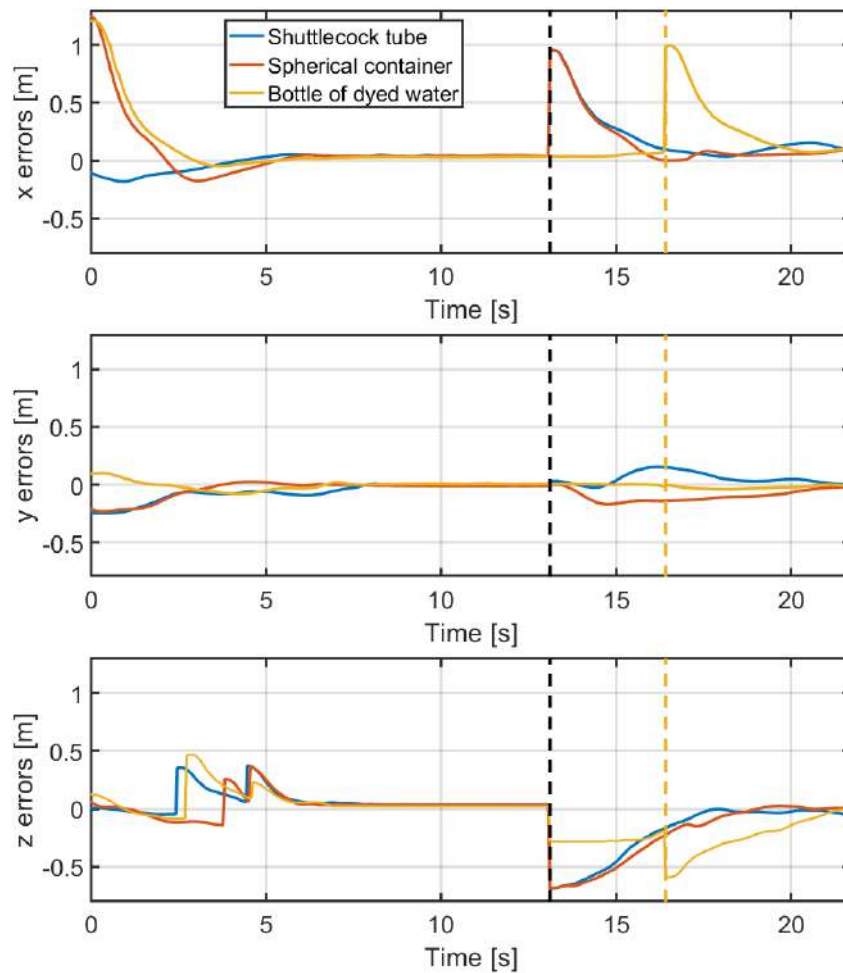


Figure 4.18: Position tracking errors during the process of grasping the three different target objects (the dotted lines depict the time of SAV started to lift the objects after grasping).

In contrast to grasping cylindrical or spherical objects, an additional setpoint was

added for grasping the rectangular bottle containing non-static dyed water to ensure a secure grip. Therefore, the SAV first grasped the bottle with dyed water and hovered at a height of 0.6 m, then started flying to the desired holding location at 16.4 s. Since the SAV was instructed to fly point-to-point, the grasp time of each trial differs. The SAV took less than 22 seconds to bring the objects to the desired location due to the accuracy of the disturbance observer.

Fig. 4.19 displays the estimated disturbances for three objects during the grasping process. Notably, the spherical container (weighing 161 g) was the heaviest among the three objects, resulting in the largest estimated disturbance magnitude along the z-axis (d_{W_z}), approximately -1, when grasped by the SAV. The other two objects' magnitudes of d_{W_z} are similar and slightly less than that of the spherical container due to their comparable weights (110 g and 113 g). These results indicate that the proposed observer can estimate the disturbance induced by the non-static mass. Besides, the dynamic changes during the SAV aerial grasping are crucially influenced by the increased mass created by the target objects, which is under the SAV. Hence, the changes in d_{W_x} and d_{W_y} are not as strong as those in d_{W_z} . These findings indicate that the proposed observer is capable of evaluating the disturbances by both static and non-static masses.

Note that the dotted lines in Fig. 4.18 and Fig. 4.19 presented the time of SAV started to lift the objects after grasping the objects. For the plastic bottle with dyed water, the SAV first lifted it at 0.6 m and remained hovering at the x and y positions of the grasping point for around 3 seconds (black dotted line). Then, the SAV brought the bottle to reach 1 m altitude (yellow dotted line). For the shuttlecock tube and spherical container, the SAV lifted them once to reach 1 m altitudes (black dotted line), respectively.

After collecting the experimental results of those three aerial grasping tasks, their success rate is presented in Table 4.2. For each trial, the battery of SAV is fully charged to neglect the disturbance from battery dearth. Despite its relatively high weight, the spherical container with a load was successfully grasped in all trials, attributable to the

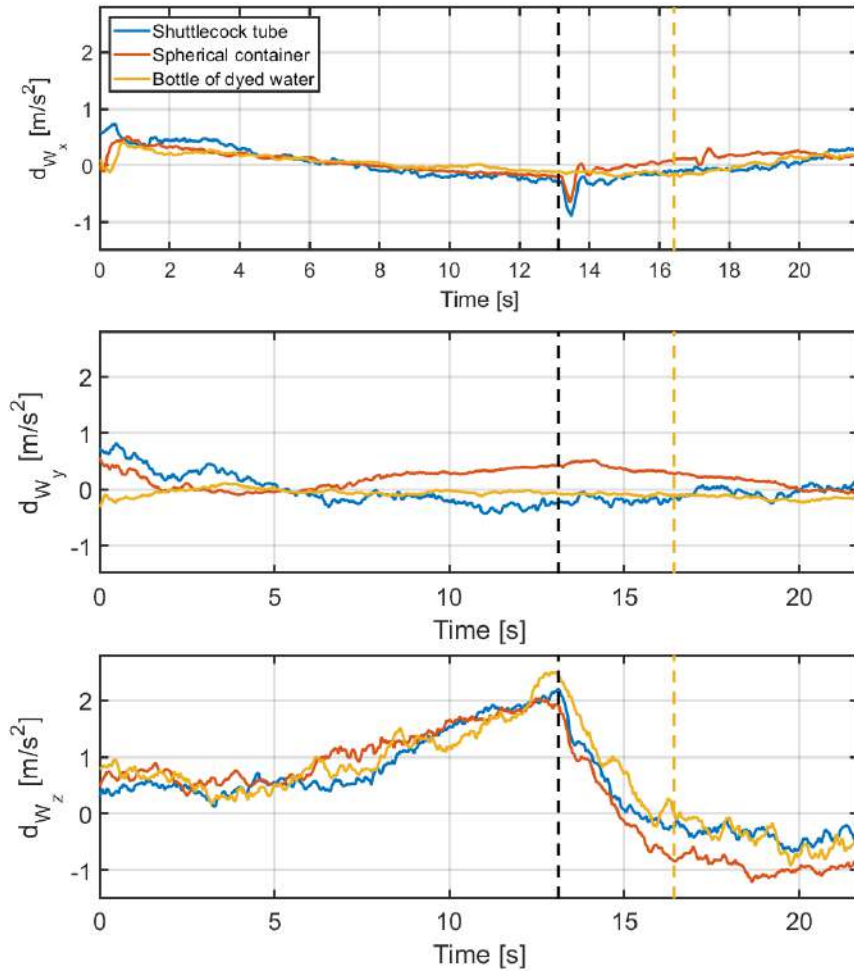


Figure 4.19: Disturbance results from grasping the three different target objects (the dotted lines depict the time of SAV started to lift the objects after grasping).

Table 4.2: Comparison of SAV aerial grasping performance with the three target objects.

Configurations	Target objects	Successes
H-base	Shuttlecock Tube with 46 g load	27/30(90%)
X-base	Spherical container with 118 g load	30/30(100%)
H-base	Plastic bottle with 80 g dyed water	20/30(66.7%)

soft gripper's tolerance. The grasping tolerance-to-objects' surface ratio in the spherical container grasping task was the highest. However, although the weights of the bottle containing dyed water and the shuttlecock tube containing the load were similar, the success rate for gripping the bottle was significantly lower compared to that of the shuttlecock tube. This discrepancy can be attributed to the rectangular shape of the plastic bottle, which requires higher pinching forces from the soft finger. As a result, although the SAV consistently achieved successful reachability to the bottle, it may struggle to lift it due to the limited contact area between the soft fingertips and the lateral surface of the bottle. Consequently, the success rate for grasping the plastic bottle with dyed water was the lowest, while the success rate for grasping the spherical container with load was the highest.

4.8 Soft Landing Test

As mentioned in Section 1.3, the proposed soft gripper of the Soft aerial vehicle (SAV) also serves as a soft landing gear to improve the flight efficiency of aerial manipulation without burdening the payload capability. The soft gripper replaces the traditional rigid one for decreasing the net weight of the SAV and simplifying the SAV's mechanism. The soft gripper establishes its landing ability by keeping a full opening as a soft landing gear to stabilize the pose of the SAV and dampen the impact forces during landing. The landing pressure is the same as the deflation pressure during grasping. Thus, the suggested soft landing does not require any extra cost of the soft gripper's control.

4.8.1 Results of Soft Gripper Without Inextensible Layers

According to [32], in Fig. 4.20 (a) and (b), with a modular soft gripper of no inextensible layer, this novel SAV can take off and land on the ground without the need for traditional rigid landing gear. Since the landing pressure is equivalent to the deflation pressure used during grasping, the soft gripper can remain fully opened, serving as a landing gear to stabilize the pose of the SAV during takeoff and effectively dampen impact forces upon landing. Besides, Fig. 4.20 (c) and Fig. 4.20(d) present the successful tilt landing of the SAV (with its two configurations of the soft gripper) on a 10° inclined platform. According to Table 4.3, the H-base soft gripper performs better for the tilt landing as it can always be flattened, while the X-base soft gripper sometimes may only have three fingers to be flattened and even jump out from the platform due to the impact forces. These tilt landing results show that the H-base soft gripper can dampen the impact forces of the soft fingers more since the fingers have more contact areas with the tilted platform. Thus, the modular soft gripper can successfully replace conventional rigid landing gear, even for tilt landing.

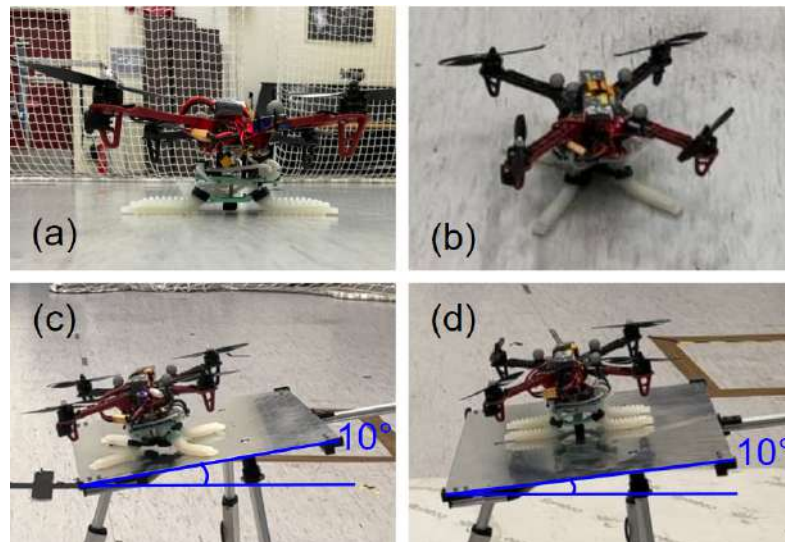


Figure 4.20: Standard landing test with (a) the H-base soft gripper and (b) the X-base soft gripper, and tilt landing test with the (c) X-base and (d) H-base soft gripper.

Table 4.3: Comparison of SAV landing performance on ground and tilt platform.

Configurations	Successes (ground)	Successes (tilt)
X-base	10/10(100%)	6/10(60%)
H-base	10/10(100%)	10/10(100%)

4.8.2 Results of Soft Gripper With Inextensible Layers

As the soft landing gear in [32] cannot get 100 % success rate of its tilt landing with X-base soft gripper, the four arms of the airframe in [38] extend for protecting the brushless motors in case that the SAV cannot land with its four soft fingers flatly on the ground or any tilted surfaces. In Fig. 4.21 (a) and (b) describe the standard soft landing of the SAV with its soft gripper that contains inextensible layers. The standard soft landing performance is similar to that in Fig. 4.20. Moreover, the SAV in Fig. 4.21 (c) and (d) demonstrate the soft landing with just two soft fingers and the assistance of the two arms of its airframe. This approach can protect the brushless motors even if the SAV cannot land with all four soft fingers.

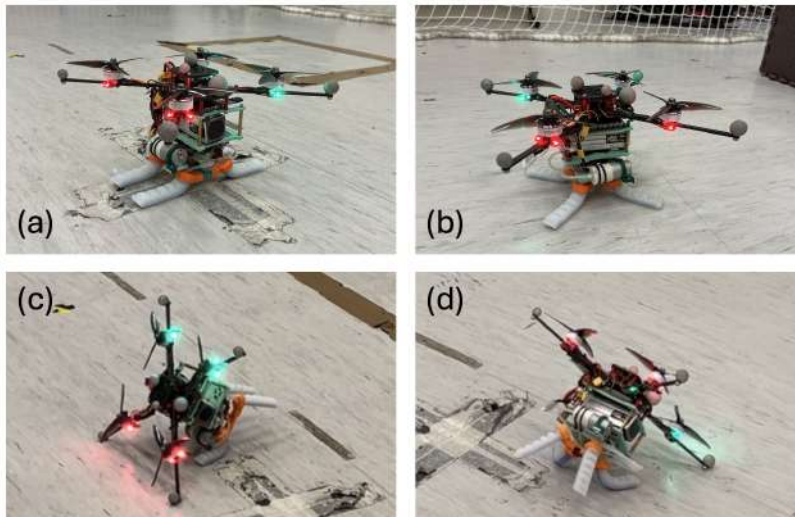


Figure 4.21: Standard landing with (a) the H-base soft gripper and (b) the X-base soft gripper, and landing with two soft fingers of the (c) H-base and (d) X-base soft gripper.

Chapter 5

Conclusion and Future Work

5.1 Conclusion

In conclusion, this thesis has presented the design and control of a novel Soft aerial vehicle (SAV) with a modular pneumatic soft gripper to conduct autonomous aerial grasping in an indoor environment. Not only considering the grasping and tracking performance during aerial grasping, but the SAV also contribute to the soft landing with its deflated soft gripper. These findings contribute to developing autonomous aerial grasping capabilities in soft robotic systems.

The first section presents the design and control of a modular pneumatic soft gripper [32]. The main objective of this soft gripper design is to maintain a lightweight structure, thereby minimizing the impact on the flight capabilities of the SAV. Therefore, the proposed soft gripper weighs a maximum of 270 g (with inextensible layers) and a minimum of 252 g (H-base without inextensible layers). Pressure control for the modular gripper utilizes a feed-forward proportional controller to improve pressure regulation. Experimental results from grasping tests reveal that the total contact areas of the gripper on the target object influence the grasping force. Two base configurations for the modular soft gripper are explored to accommodate objects of different shapes. The H-base 4-tip

gripper is suitable for cylindrical or rectangular objects, while the X-base 4-tip gripper is more appropriate for spherical or rounded objects.

Subsequently, a Disturbance observer-based nonlinear model predictive control (DOMPC) system for soft aerial grasping with the SAV is proposed [38]. By incorporating a disturbance observer and utilizing Extended Kalman filter (EKF), this method can adapt to dynamic model changes and handle unpredictable disturbances throughout the aerial grasping task. The DOMPC compensates for uncertainties arising from payload weight variations and other external disturbances, such as battery discharging. The SAV equipped with DOMPC demonstrates the capability to handle both static and non-static payloads. It can automatically grasp an 80 g dyed water-filled plastic bottle, even when the dyed water is shaking, inducing unestimated disturbances. Furthermore, the 270 g lightweight, soft gripper, combined with a 732 g customized traditional quadrotor, achieves successful mid-air grasping of various objects, including a plastic box (337 g) in the payload test and a spherical container (160 g) in the aerial grasping test. The payload-to-weight ratio achieved by the SAV surpasses previous investigations on soft grasping, highlighting its effectiveness.

Lastly, this thesis demonstrates successful soft landing tasks on the ground and a tilted platform with a ten-degree inclined angle [32, 38]. The proposed soft gripper is equipped under a conventional quadrotor as a novel SAV to conduct the aerial grasping and landing operation. In the landing test, the soft gripper efficiently replaced the traditional rigid landing gear when it deflated. This soft landing approach simplifies the control complexity for landing for the Unmanned aerial vehicle (UAV) with its gripper.

5.2 Future works

In future, to further contribute to the drone delivery industry, the proposed Soft aerial vehicle (SAV) aims to grasp some common rubbish at the seacoast and the country parks,

such as aluminium cans, plastic bottles, polystyrene pieces, and boxes that can contain first aid kits for the search and rescue of the hiking accidents in Hong Kong. For the above application, object detection [77, 78] should be developed so the SAV will require more sensors to navigate itself outdoors. Hence, the outdoor target objects of the SAV can be recognized without the position feedback of the indoor motion capture system.

For the outdoor localization of the SAV itself, a low-cost real time kinematics (RTK) Global navigation satellite system (GNSS) can be used [79, 80]. Enhancing the autonomous flight safety of the Unmanned aerial vehicle (UAV) can be achieved by improving outdoor trajectory control using object detection and RTK GNSS technology. According to the previous proactive landing approach [76], the localization of the drone and its destination can also be defined by a sensor-fusion and estimation method from ArUco marker, YOLO object detector [81], stereo depth information from dual camera, and drone's Initial measurement unit (IMU) information.

Chapter 6

Appendices

6.1 Video of Static Grasping



Figure 6.1: QR code for the video of the static grasping test by the soft gripper.

Link: <https://youtu.be/v6xmPBTzEkY>

6.2 Video of Payload Test



Figure 6.2: QR code for the video of SAV's payload test.

Link: <https://youtu.be/01u3tZnKE7Y>

6.3 Video of Aerial Grasping



Figure 6.3: QR code for the SAV's aerial grasping test video.

Link: https://youtu.be/kD9XIhZy_TA

6.4 Video of Soft Landing



Figure 6.4: QR code for the video of soft landing.

Link: <https://youtu.be/ZCXvp52NnWo>

6.5 Open-source Materials (GitHub)

- DOMPC
- Feed-forward Proportional control of the modular pneumatic soft gripper
- Moulds for soft gripper with an inextensible layer
- Moulds of soft gripper without inextensible layer

Bibliography

- [1] T. Hassan, M. Manti, G. Passetti, N. d'Elia, M. Cianchetti, and C. Laschi, "Design and development of a bio-inspired, under-actuated soft gripper," in *2015 37th Annual International Conference of the IEEE Engineering in Medicine and Biology Society (EMBC)*. IEEE, 2015, pp. 3619–3622.
- [2] P. Ramon-Soria, A. E. Gomez-Tamm, F. J. Garcia-Rubiales, B. C. Arrue, and A. Ollero, "Autonomous landing on pipes using soft gripper for inspection and maintenance in outdoor environments," in *2019 IEEE/RSJ International Conference on Intelligent Robots and Systems (IROS)*. IEEE, 2019, pp. 5832–5839.
- [3] J. Fishman, S. Ubellacker, N. Hughes, and L. Carlone, "Dynamic grasping with a soft drone: From theory to practice," in *2021 IEEE/RSJ International Conference on Intelligent Robots and Systems (IROS)*. IEEE, 2021, pp. 4214–4221.
- [4] S. Ubellacker, A. Ray, J. M. Bern, J. Strader, and L. Carlone, "High-speed aerial grasping using a soft drone with onboard perception," *npj Robotics*, vol. 2, no. 1, p. 5, 2024.
- [5] Z. Liu, C. Mucchiani, K. Ye, and K. Karydis, "Safely catching aerial micro-robots in mid-air using an open-source aerial robot with soft gripper," *Frontiers in Robotics and AI*, vol. 9, p. 1030515, 2022.

- [6] A. Shtarbanov, “Flowio development platform—the pneumatic “raspberry pi” for soft robotics,” in *Extended abstracts of the 2021 CHI conference on human factors in computing systems*, 2021, pp. 1–6.
- [7] J. T. Ping, B. H. Khoo, O. A. Syadiqeen, N. Khoo, C. P. Tan, and S. G. Nurzaman, “Aerial grasping by a quadrotor uav with a soft material gripper,” 2020.
- [8] D. Sarkar, A. Arora, S. Sen, S. S. Katta, D. Shashank, M. Rohan, and S. Saha, “Development of an autonomous uav integrated with a manipulator and a soft gripper,” in *2022 13th Asian Control Conference (ASCC)*. IEEE, 2022, pp. 2212–2217.
- [9] A. Kumar and L. Behera, “Design, localization, perception, and control for gps-denied autonomous aerial grasping and harvesting,” *IEEE Robotics and Automation Letters*, vol. 9, no. 4, pp. 3538–3545, 2024.
- [10] W. R. Roderick, M. R. Cutkosky, and D. Lentink, “Bird-inspired dynamic grasping and perching in arboreal environments,” *Science Robotics*, vol. 6, no. 61, p. eabj7562, 2021.
- [11] J. Thomas, G. Loianno, J. Polin, K. Sreenath, and V. Kumar, “Toward autonomous avian-inspired grasping for micro aerial vehicles,” *Bioinspiration & biomimetics*, vol. 9, no. 2, p. 025010, 2014.
- [12] N. Bucki, J. Tang, and M. W. Mueller, “Design and control of a midair-reconfigurable quadcopter using unactuated hinges,” *IEEE Transactions on Robotics*, vol. 39, no. 1, pp. 539–557, 2022.
- [13] C. Eschmann, “Unmanned aircraft systems for remote building inspection and monitoring,” 2012.

- [14] S. Qazi, A. S. Siddiqui, and A. I. Wagan, "Uav based real time video surveillance over 4g lte," in *2015 International Conference on Open Source Systems & Technologies (ICOSST)*. IEEE, 2015, pp. 141–145.
- [15] W.-C. Chiang, Y. Li, J. Shang, and T. L. Urban, "Impact of drone delivery on sustainability and cost: Realizing the uav potential through vehicle routing optimization," *Applied energy*, vol. 242, pp. 1164–1175, 2019.
- [16] J. Sun, B. Li, Y. Jiang, and C.-y. Wen, "A camera-based target detection and positioning uav system for search and rescue (sar) purposes," *Sensors*, vol. 16, no. 11, p. 1778, 2016.
- [17] J. F. Elfferich, D. Dodou, and C. Della Santina, "Soft robotic grippers for crop handling or harvesting: A review," *IEEE Access*, vol. 10, pp. 75 428–75 443, 2022.
- [18] C. W. Chang, "Proactive guidance for accurate quadrotor-based uav landing on dynamic platform," Ph.D. dissertation, Hong Kong Polytechnic University, 2022.
- [19] G. Muchiri and S. Kimathi, "A review of applications and potential applications of uav," in *Proceedings of the Sustainable Research and Innovation Conference*, 2022, pp. 280–283.
- [20] C. A. Thiels, J. M. Aho, S. P. Zietlow, and D. H. Jenkins, "Use of unmanned aerial vehicles for medical product transport," *Air medical journal*, vol. 34, no. 2, pp. 104–108, 2015.
- [21] S. Yeong, L. King, and S. Dol, "A review on marine search and rescue operations using unmanned aerial vehicles," *International Journal of Marine and Environmental Sciences*, vol. 9, no. 2, pp. 396–399, 2015.

-
- [22] J. Qi, J. Kang, and X. Lu, “Design and research of uav autonomous grasping system,” in *2017 IEEE International Conference on Unmanned Systems (ICUS)*. IEEE, 2017, pp. 126–131.
- [23] C. A. Department, “Small unmanned aircraft order (cap.448g),” 2022.
- [24] H. B. Khamseh, F. Janabi-Sharifi, and A. Abdessameud, “Aerial manipulation—a literature survey,” *Robotics and Autonomous Systems*, vol. 107, pp. 221–235, 2018.
- [25] H. Lipson, “Challenges and opportunities for design, simulation, and fabrication of soft robots,” *Soft Robotics*, vol. 1, no. 1, pp. 21–27, 2014.
- [26] D. Rus and M. T. Tolley, “Design, fabrication and control of soft robots,” *Nature*, vol. 521, no. 7553, pp. 467–475, 2015.
- [27] S. Kim, C. Laschi, and B. Trimmer, “Soft robotics: a bioinspired evolution in robotics,” *Trends in biotechnology*, vol. 31, no. 5, pp. 287–294, 2013.
- [28] V. Spurný, T. Báča, M. Saska, R. Pěnička, T. Krajník, J. Thomas, D. Thakur, G. Loianno, and V. Kumar, “Cooperative autonomous search, grasping, and delivering in a treasure hunt scenario by a team of unmanned aerial vehicles,” *Journal of Field Robotics*, vol. 36, no. 1, pp. 125–148, 2019.
- [29] H. Chen, F. Quan, L. Fang, and S. Zhang, “Aerial grasping with a lightweight manipulator based on multi-objective optimization and visual compensation,” *Sensors*, vol. 19, no. 19, p. 4253, 2019.
- [30] R. Spica, A. Franchi, G. Oriolo, H. H. Bühlhoff, and P. R. Giordano, “Aerial grasping of a moving target with a quadrotor uav,” in *2012 IEEE/RSJ International Conference on Intelligent Robots and Systems*. IEEE, 2012, pp. 4985–4992.
- [31] J. Thomas, J. Polin, K. Sreenath, and V. Kumar, “Avian-inspired grasping for quadrotor micro uavs,” in *International Design Engineering Technical Conferences*

- and Computers and Information in Engineering Conference*, vol. 55935. American Society of Mechanical Engineers, 2013, p. V06AT07A014.
- [32] H. C. Cheung, C.-W. Chang, B. Jiang, C.-Y. Wen, and H. K. Chu, “A modular pneumatic soft gripper design for aerial grasping and landing,” in *2024 IEEE 7th International Conference on Soft Robotics (RoboSoft)*. IEEE, 2024, pp. 82–88.
- [33] W. Zhou, K. Yin, R. Wang, Y.-E. Wang *et al.*, “Design of attitude control system for uav based on feedback linearization and adaptive control,” *Mathematical Problems in Engineering*, vol. 2014, 2014.
- [34] M. Schreier, “Modeling and adaptive control of a quadrotor,” in *2012 IEEE international conference on mechatronics and automation*. IEEE, 2012, pp. 383–390.
- [35] G. Chen, J. Zhou, L. Wang, Y. Wang, Y. Yin, and Z. Ding, “Modeling and adaptive controlling of quadrotor uav with flexible gripper,” in *2022 IEEE 10th Joint International Information Technology and Artificial Intelligence Conference (ITAIC)*, vol. 10. IEEE, 2022, pp. 1984–1991.
- [36] M. Liu, F. Zhang, and S. Lang, “The quadrotor position control based on mpc with adaptation,” in *2021 40th Chinese Control Conference (CCC)*, 2021, pp. 2639–2644.
- [37] M. Kamel, T. Stastny, K. Alexis, and R. Siegwart, “Model predictive control for trajectory tracking of unmanned aerial vehicles using robot operating system,” in *Robot Operating System (ROS): The Complete Reference (Volume 2)*. Springer International Publishing, 2017, pp. 3–39.
- [38] H. C. Cheung, B. Jiang, Y. Hu, H. K. Chu, C.-Y. Wen, and C.-W. Chang, “Aerial grasping with soft aerial vehicle using disturbance observer-based model predictive control,” 2024. [Online]. Available: <https://arxiv.org/abs/2409.14115>

-
- [39] B. Jiang, B. Li, W. Zhou, L.-Y. Lo, C.-K. Chen, and C.-Y. Wen, “Neural network based model predictive control for a quadrotor uav,” *Aerospace*, vol. 9, no. 8, p. 460, 2022.
- [40] B. Li, W. Zhou, J. Sun, C.-Y. Wen, and C.-K. Chen, “Development of model predictive controller for a tail-sitter vtol uav in hover flight,” *Sensors*, vol. 18, no. 9, p. 2859, 2018.
- [41] Y. Zhu, X. He, P. Zhang, G. Guo, and X. Zhang, “Perching and grasping mechanism inspired by a bird’s claw,” *Machines*, vol. 10, no. 8, p. 656, 2022.
- [42] J. P. King, D. Bauer, C. Schlangenhaus, K.-H. Chang, D. Moro, N. Pollard, and S. Coros, “Design, fabrication, and evaluation of tendon-driven multi-fingered foam hands,” in *2018 IEEE-RAS 18th International Conference on Humanoid Robots (Humanoids)*. IEEE, 2018, pp. 1–9.
- [43] M. Manti, T. Hassan, G. Passetti, N. D’Elia, C. Laschi, and M. Cianchetti, “A bioinspired soft robotic gripper for adaptable and effective grasping,” *Soft Robotics*, vol. 2, no. 3, pp. 107–116, 2015.
- [44] J. Fishman and L. Carlone, “Control and trajectory optimization for soft aerial manipulation,” in *2021 IEEE Aerospace Conference (50100)*. IEEE, 2021, pp. 1–17.
- [45] I. Smooth-On, “Flexfoam-it! x.” Smooth-On, Inc, Tech. Rep., 2024.
- [46] —, “Dragon skin 30 product information,” Smooth-On, Inc, Tech. Rep., 2024.
- [47] R. Peng, Z. Wang, and P. Lu, “Aecom: An aerial continuum manipulator with precise kinematic modeling for variable loading and tendon-slacking prevention,” *arXiv preprint arXiv:2110.14180*, 2021.

- [48] J. L. Chien, C. Leong, J. Liu, and S. Foong, “Design and control of an aerial-ground tethered tendon-driven continuum robot with hybrid routing,” *Robotics and Autonomous Systems*, vol. 161, p. 104344, 2023.
- [49] G. Phanomchoeng, P. Pitchayawetwongsa, N. Boonchumanee, S. Lin, and R. Chanchaen, “Grasping profile control of a soft pneumatic robotic gripper for delicate gripping,” *Robotics*, vol. 12, no. 4, p. 107, 2023.
- [50] H. Zhang, W. Liu, M. Yu, and Y. Hou, “Design, fabrication, and performance test of a new type of soft-robotic gripper for grasping,” *Sensors*, vol. 22, no. 14, p. 5221, 2022.
- [51] A. Kumar and L. Behera, “Thrust microstepping via acceleration feedback in quadrotor control for aerial grasping of dynamic payload,” *IEEE Robotics and Automation Letters*, vol. 9, no. 2, 2024.
- [52] P. E. Pounds, D. R. Bersak, and A. M. Dollar, “The yale aerial manipulator: grasping in flight,” in *2011 IEEE International Conference on Robotics and Automation*. IEEE, 2011, pp. 2974–2975.
- [53] P. Kremer, H. R. Nohooji, J. L. Sanchez-Lopez, and H. Voos, “A lightweight universal gripper with low activation force for aerial grasping,” *arXiv preprint arXiv:2208.10768*, 2022.
- [54] F. Ruiz, B. C. Arrue, and A. Ollero, “Sophie: Soft and flexible aerial vehicle for physical interaction with the environment,” *IEEE Robotics and Automation Letters*, vol. 7, no. 4, pp. 11 086–11 093, 2022.
- [55] H. Hsiao, F. Wu, J. Sun, and J. Zhao, “A novel passive mechanism for flying robots to perch onto surfaces,” in *2022 International Conference on Robotics and Automation (ICRA)*. IEEE, 2022, pp. 1183–1189.

- [56] S. Ubellacker, “Grasping static and moving targets with a soft drone: Control and prediction,” 2021.
- [57] J. Fishman, “Soft aerial manipulation,” 2021.
- [58] D. Mellinger and V. Kumar, “Minimum snap trajectory generation and control for quadrotors,” in *2011 IEEE international conference on robotics and automation*. IEEE, 2011, pp. 2520–2525.
- [59] S. Ubellacker, A. Ray, J. Bern, J. Strader, and L. Carlone, “Aggressive aerial grasping using a soft drone with onboard perception,” *arXiv preprint arXiv:2308.06351*, 2023.
- [60] C. Tawk, R. Mutlu, and G. Alici, “A 3d printed modular soft gripper integrated with metamaterials for conformal grasping,” *Frontiers in Robotics and AI*, vol. 8, p. 799230, 2022.
- [61] Z. Wang, Y. Torigoe, and S. Hirai, “A prestressed soft gripper: design, modeling, fabrication, and tests for food handling,” *IEEE Robotics and Automation Letters*, vol. 2, no. 4, pp. 1909–1916, 2017.
- [62] J. Zhang, A. Jackson, N. Mentzer, and R. Kramer, “A modular, reconfigurable mold for a soft robotic gripper design activity,” *Frontiers in Robotics and AI*, vol. 4, p. 46, 2017.
- [63] Y. Zhao and Y. Wang, “A palm-shape variable-stiffness gripper based on 3d-printed fabric jamming,” *IEEE Robotics and Automation Letters*, vol. 8, no. 6, pp. 3238–3245, 2023.
- [64] M. Yu, W. Liu, J. Zhao, Y. Hou, X. Hong, and H. Zhang, “Modeling and analysis of a composite structure-based soft pneumatic actuators for soft-robotic gripper,” *Sensors*, vol. 22, no. 13, p. 4851, 2022.

- [65] W. Wenjie, H. Zhen, C. Rui, J. Feiteng, and S. Huiming, "Trajectory tracking control design for uav based on mpc and active disturbance rejection," in *2018 IEEE CSAA Guidance, Navigation and Control Conference (CGNCC)*, 2018, pp. 1–5.
- [66] D. Yan, W. Zhang, H. Chen, and J. Shi, "Robust control strategy for multi-uavs system using mpc combined with kalman-consensus filter and disturbance observer," *ISA Transactions*, vol. 135, pp. 35–51, 2023. [Online]. Available: <https://www.sciencedirect.com/science/article/pii/S0019057822004797>
- [67] B. Zhang, X. Sun, S. Liu, and X. Deng, "Tracking control of multiple unmanned aerial vehicles incorporating disturbance observer and model predictive approach," *Transactions of the Institute of Measurement and Control*, vol. 42, no. 5, pp. 951–964, 2020.
- [68] Y. Hu, B. Li, B. Jiang, J. Han, and C.-Y. Wen, "Disturbance observer-based model predictive control for an unmanned underwater vehicle," *Journal of Marine Science and Engineering*, vol. 12, no. 1, p. 94, 2024.
- [69] D. Hanover, P. Foehn, S. Sun, E. Kaufmann, and D. Scaramuzza, "Performance, precision, and payloads: Adaptive nonlinear mpc for quadrotors," *IEEE Robotics and Automation Letters*, vol. 7, no. 2, pp. 690–697, 2021.
- [70] Y. Yang, T. Huang, T. Wang, and C.-y. Wen, "A robust sliding-mode control framework for quadrotors subject to model uncertainty and external disturbances," in *Proceedings of the 2024 American Control Conference*, 2024.
- [71] M. I. Ribeiro, "Kalman and extended kalman filters: Concept, derivation and properties," *Institute for Systems and Robotics*, vol. 43, no. 46, pp. 3736–3741, 2004.
- [72] J. H. Lee and N. L. Ricker, "Extended kalman filter based nonlinear model predictive control," *Industrial & Engineering Chemistry Research*, vol. 33, no. 6, pp. 1530–1541, 1994.

-
- [73] Y. Yang, X. Ban, H. Lu, T. Huang, and X. Huang, “Parameter optimization for a quadrotor system with external disturbance and uncertainty via reinforcement learning,” in *Chinese Control Conference (CCC 2024)*. IEEE, 2024.
- [74] D. Yan, W. Zhang, H. Chen, and J. Shi, “Robust control strategy for multi-uavs system using mpc combined with kalman-consensus filter and disturbance observer,” *ISA transactions*, vol. 135, pp. 35–51, 2023.
- [75] R. Verschueren, G. Frison, D. Kouzoupis, J. Frey, N. v. Duijkeren, A. Zanelli, B. Novoselnik, T. Albin, R. Quirynen, and M. Diehl, “acados—a modular open-source framework for fast embedded optimal control,” *Mathematical Programming Computation*, vol. 14, no. 1, pp. 147–183, 2022.
- [76] C.-W. Chang, L.-Y. Lo, H. C. Cheung, Y. Feng, A.-S. Yang, C.-Y. Wen, and W. Zhou, “Proactive guidance for accurate uav landing on a dynamic platform: A visual-inertial approach,” *Sensors*, vol. 22, no. 1, p. 404, 2022.
- [77] Z. Chen, C. Wang, H. Wang, P. Li, Y. Li, and X. Wu, “Object detection for uav grasping: Solution and analysis,” in *2018 IEEE International Conference on Information and Automation (ICIA)*. IEEE, 2018, pp. 1078–1083.
- [78] A. Kumar, M. Vohra, R. Prakash, and L. Behera, “Towards deep learning assisted autonomous uavs for manipulation tasks in gps-denied environments,” in *2020 IEEE/RSJ International Conference on Intelligent Robots and Systems (IROS)*. IEEE, 2020, pp. 1613–1620.
- [79] W. Stempfhuber and M. Buchholz, “A precise, low-cost rtk gnss system for uav applications,” *The International Archives of the Photogrammetry, Remote Sensing and Spatial Information Sciences*, vol. 38, pp. 289–293, 2012.
- [80] Y. Matsuura, Z. Heming, K. Nakao, C. Qiong, I. Firmansyah, S. Kawai, Y. Yamaguchi, T. Maruyama, H. Hayashi, and H. Nobuhara, “High-precision plant height

measurement by drone with rtk-gnss and single camera for real-time processing,”
Scientific Reports, vol. 13, no. 1, p. 6329, 2023.

- [81] Y. Feng, K. Tse, S. Chen, C.-Y. Wen, and B. Li, “Learning-based autonomous uav system for electrical and mechanical (e&m) device inspection,” *Sensors*, vol. 21, no. 4, p. 1385, 2021.